International Journal of Hydrogen Energy 58 (2024) 1160–1176

Contents lists available at ScienceDirect

International Journal of Hydrogen Energy

journal homepage: www.elsevier.com/locate/he

Energy analysis of a power-to-jet-fuel plant

J.H. Boilley [a,b], A. Berrady [b], H. Bin Shahrel [b], E. Gürbüz [b], F. Gallucci [a,*]

[a] Sustainable Process Engineering, Chemical Engineering and Chemistry, Eindhoven University of Technology, Eindhoven, the Netherlands
[b] Hydrogen Lab ENGIE LAB CRIGEN, 4 Rue Joséphine Baker, 93240, Stains, France

ARTICLE INFO

Handling Editor: Søren Juhl Andreasen

Keywords:
Power-to-fuels
Hydrogen
Energy analysis
Synthetic fuels
Carbon capture and utilisation
Fischer-tropsch
SOEC

ABSTRACT

Sustainable aviation fuel (SAF) production from captured carbon dioxide and green hydrogen, is referred to as the key to decarbonize the hard-to-abate aviation sector. Fischer-Tropsch is a mature and reliable pathway for hydrocarbon synthesis, with a wide spectrum of technological options and high plant efficiency extending to more than 80 % of e-kerosene selectivity. In this work, an Aspen Hysys model, coupled with different Matlab simulations for Fischer-Tropsch, Hydrocracker and SOEC, was set up to estimate efficiency and selectivity. The results show that global efficiency is mainly linked to the efficiency of the production of H_2. Energetic efficiency reaches 48.06 % using the already existing commercial electrolyte supported cell in a SOEC electrolyser, but it could increase to 65.74 % if cathode supported cell was considered.

1. Introduction

Since the Paris agreement after COP21, increasing efforts have been made in order to decrease GHG emissions and to reduce the impact of climate change below 1.5 °C compared to 1990 [1]. Reaching this goal of 1.5 °C corresponds to a 45 % net decrease of emissions in 2030 compared to 2010 and net zero in 2050 [2]. The energy transition from fossil fuels to renewable sources is a crucial factor in reducing greenhouse gas emissions. This transition can be implemented at various stages of the value chain, depending on the specific sector of use. In 2010, the direct emissions from mobility were approximately 7 Gt per year, which corresponds to 23 % of total emissions in 2014 [3], and 27 % of European emissions [4]. The switching from non-renewable energy sources will directly impact the existing infrastructure by developing technologies based on batteries (electric cars, buses, etc.) or hydrogen. While this change does not require a radical change in the end-user mobility system (e.g. electric vehicles), in the *hard-to-abate* sector (marine, aviation and heavy-duty vehicles) the switching from fossil fuel to renewable energy poses a harder challenge [5]. The civil aviation sector has become increasingly accessible due to the availability of a larger fleet of airplanes, reduced fuel consumption, and the introduction of an economy class, contributing to approximately 3 % of the global CO2 emissions and generating an annual output of 814 billion tons [6], in addition to this and according to the IATA (International Air Transport Association) it is expected that the air transport will face an increase of demand by 4.5 % [7]. Moreover, even assuming a highly optimistic integration of hydrogen and electric solutions, 80 % of energy demand for aviation will still depend on hydrocarbons in 2050 [8]. Considering all the mentioned aspects, a decarbonization of aviation fuel is mandatory to respect Paris agreement.

ICAO designates by Alternative Aviation Fuels (*AAF),* all the fuels of non-petroleum origin (coal, gases, biomass, etc.), which can be considered Sustainable Aviation Fuel (SAF) if they meet sustainable criteria. SAFs have a limited impact on GHG: according to the REDII directives from European Union, an alternative fuel could be considered as sustainable if the GHG emissions reduction are at least 65 % compared to conventional fuel since January 2021. The E.U. considered that a conventional fuel emits 89 g_{CO2}/MJ. This directive considers differently the SAF produced by green electricity. In this case, the fuel is not only sustainable, but it is a Renewable Fuels Non-Biological Origin (RFNBOs) defined as “renewable liquid and gaseous transport fuels of non-biological origin means liquid or gaseous fuels which are used in the transport sector other than biofuels or biogases, the energy source content of which is derived from renewable sources other than biomass”. For non-biological origin renewables fuel, the reduction has to be at least 70 % [9]. There are currently two pathways for e-fuel production identified, Methanol-to-Jet and the Fischer-Tropsch pathway [10], but only the latter is currently allowed by ASTM [11]. Regulations attempt to implement e-fuel through Fischer-Tropsch, for example, the European Commission proposed in 2021 a mandate for blending e-fuel for 2025.

In a power to jet fuel plant, the CO_2 is the only source of carbon in the

* Corresponding author.
E-mail address: f.gallucci@tue.nl (F. Gallucci).

https://doi.org/10.1016/j.ijhydene.2024.01.262
Received 8 August 2023; Received in revised form 18 January 2024; Accepted 21 January 2024
Available online 31 January 2024

Abbreviations and nomenclature

SOEC	Solid Oxide Electrolyser Cell
FT	Fischer-Tropsch
PtL	Power-to-Liquid
MT	Mass Transfer
Act	Activation
rWGS	Reverse Water Gas Shift
LPG	Liquefied Petroleum Gas
SBR	Slurry Bubble Reactor
ASF	Anderson-Schultz-Flory
ASTM	American Society for Testing and Material
HCC	Hydrocracker
LHV	Lower Heating Value (MWh/ton)
U	Cell voltage (V)
η	Overpotential losses (V)
ASR	Area Specific Resistance (Ω/cm^2)
Deg	Degradation rate (%)
ESC	Electrolyte-Supported Cell
CSC	Cathode-Supported Cell
j	local current density (A/m^2)
Far	Faraday's Constant (C/mol)
$\overline{R}$	Ideal Gas Constant (J/(mol K))
ν_i	Stochiometric coefficient of gas species i
A	Area of the cell (m^2)
$\dot{Q}$	Date of heat flow (W)
ΔH^0_{298}	Standard enthalpy of reaction (J/mol)
Δh	Enthalpy of reaction (J/mol)
$\dot{M}_i$	Mass flow of product i (ton/h)
R	Reaction rate (mol/(s m^2))
α	Growth Coefficient
T	Temperature (K)
t	Operating time of the stack (s)
ϵ	Volumetric fraction
G	Gas phase
L	Liquid phase
S	Solid phase
LB	Large Bubble
SB	Small Bubble
V	Velocity (m/s)
D_L	Diffusion Coefficient in the liquid (m^2/s)
m	Partition coefficient or the solubilities
β	Contraction factor
k_La	Volumetric mass transfer coefficient (s^{-1})
C	Concentration (mol/m^3)
X	Conversion rate
F	Mole flow rate (mol/s)
H	Column height (m)
ρ	Density (kg/m^3)
r	Reaction rate (mol/(kg$_{cat}$ s))
E_a	Activation Energy (J/mol)

hydrocarbon molecules, thus it must be provided continuously at high purities. The capture and use of CO_2 is called CCU, this option is interesting in order to close the carbon cycle to reduce the carbon intensity of human activities.

The power to jet fuel installation can be divided into three main bricks: the hydrogen production unit, CO_2 capture brick, the Fischer-Tropsch synthesis unit and the product upgrading part. The production of hydrogen is realised in the electrolysis unit by dissociating water with electricity. In this study the hydrogen production is carried out by high-temperature electrolysis. Because the Fischer-Tropsch synthesis produces heat, it is possible to recycle part of it for steam production and thus reduce overall electricity consumption.

The Fischer-Tropsch synthesis allows the transformation of a synthesis gas (CO and H_2) into a mixture of hydrocarbons. It is currently mainly used to transform natural gas into more commercially attractive crude (PEARL GTL, BINTULU, etc.). The synthesis gas is converted into hydrocarbons by considering the following reaction:

$$nCO + (2n+1)H_2 \rightarrow C_nH_{2n+2} + nH_2O$$

This is the main reaction, but to a smaller extent, olefins, alcohol, and aromatic production could occur. The carbon distribution is the main reason behind the complexity of Fischer-Tropsch modelling. The ASF distribution is a tool used to represent the distribution of carbon among the products. Jet fuels are sensitive to the presence of alcohol and unsaturated molecules (production of gum). Therefore, the low temperature is more suitable for this production. For low temperature Fischer-Tropsch, manufacturers prefer to use cobalt as a catalyst than other metal alternatives (iron), because of its better kinetics.

Finally, the last important brick and that is product upgrading, indeed the crude from the synthesis can not be consumed directly by aviation, it is necessary to respect the standards of the ASTM relating to jet-fuels. To do this, a separation of the oil fractions is realised by a distillation unit. Some fractions are not recoverable, so the fractions lighter than naphtha will be reformed while the fractions heavier than kerosene will be cracked in a hydrocracker. This unit dissociates heavy hydrocarbons into lighter in presence of high partial pressure of hydrogen to avoid production of unsaturated molecules.

Several authors have previously proposed energy analyses of the Power-to-Liquid process. Nevertheless, despite being a subject of social debate in the European Parliament [12], there is currently a lack of studies that specifically address the production of e-jet-fuel from a civilian perspective, based on a review of existing literature, it appears that there are only one publication, from Roja-Michaga et al. [12], that specifically addresses the production of jet fuel in a civil perspective. From a military standpoint, Comidy et al. [13] offer an overview of jet fuel production from the nuclear reactor of an aircraft carrier, catering to military aviation requirements. Therefore, the objective of this study is to present the initial energy analysis of a Power-to-Jet-Fuel system intended for civil use, while adhering to regulatory standards. The overall efficiency of the system is provided by modelling tools, the global process is simulated on Aspen HYSYS while Fischer-Tropsch reactor, Hydrocracker and SOEC are simulated using Matlab.

2. Model description and approach

2.1. Process description and final products

Fig. 1 illustrates the process for production of jet fuel involving hydrogen production using SOEC, fuel production and the upgrading of the product. More specifically, the power to liquid process based on Fischer-Tropsch usually consists of 6 different main units: hydrogen production, CO_2 capture, reverse Water Gas Shift (to convert CO_2 into CO for the further conversion steps), Fischer-Tropsch reactor, product separation and product upgrading. For this analysis, the power consumption of the electrolyser is set at 200 MW. This corresponds roughly to the size of a large wind farm power station in Europe.

A power-to-liquid unit could produce different oil fractions [13]:

- **LPG** (<30 °C/C1 – C4): On the Fig. 1, LPG correspond to combustible gas, directly recycled gas is a mixture of unreacted syngas and LPG. Because LPG are easily reformed, reforming has been chosen for

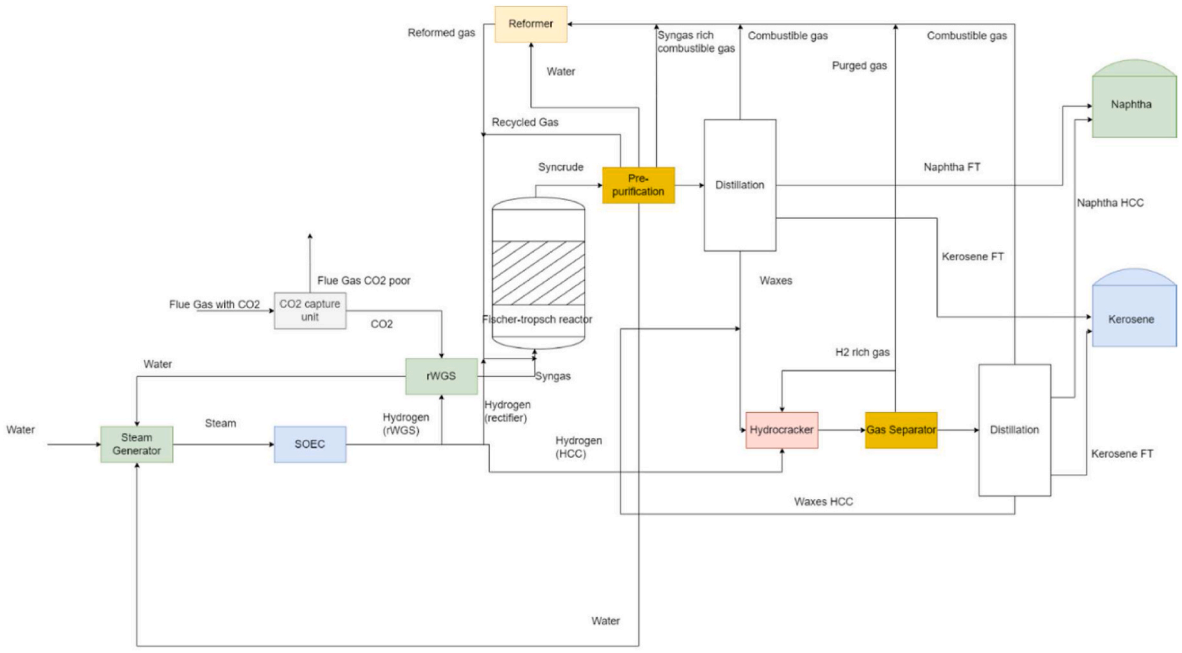

Fig. 1. Process for production of jet-fuel from green electricity, water and captured CO_2 (For interpretation of the references to colour in this figure legend, the reader is referred to the Web version of this article.)

recycling this fraction in order to increase yield of more interesting fractions.

- **Naphtha** (30–205 °C/C4 – C12): Naphtha from low-temperature Fischer-Tropsch is mostly paraffinic and thus produces gasoline with low RON and MON numbers. Therefore, Naphtha from power-to-liquid plant should be considered for its non-energy use (which includes petrochemical feedstocks, diluent for bitumen and solvents).
- **Kerosene** (180–280 °C/C9 – C18): Kerosene is the feedstock for jet-fuel. Due to its low sulphur and high paraffinic content, Fischer-Tropsch kerosene could be directly used as jet-fuel without additional unit.
- Gas oil, Vacuum gas oil and residue (**waxes**) (>121 °C/C16 – C75+): In the case of Fischer-Tropsch, all these fractions are solid at standard temperature and pressure because of their high paraffinic content (and so high H/C ratio). This fraction is called waxes and can be used in hydrocracker. Heavy fuel oil and diesel could be used in heavy transport in maritime transport but SNG, ammonia or methanol seem to be more suitable as e-fuel for this sector.

In this study, our focus is exclusively on two products: Kerosene and Naphtha, as they present the most compelling prospects for Fischer-Tropsch e-fuel. All other byproducts are effectively recycled to maximize the yield of these primary two products.

2.2. Considered chemical species and thermodynamic

The considered species in this analysis are H_2, CO, N_2, H_2O, CO_2 and paraffinic hydrocarbons from C1 to C75. Hydrocarbons with a carbon number above 30 are represented by their normal boiling point temperature which was estimated with the NIST Chemistry WebBook [14]. Until the hydrocracker, it is assumed that all the hydrocarbons are linear.

To estimate thermodynamic properties of fluids before the FT reactor, the Peng Robinson equation of state has been used. To estimate vapor liquid equilibria for fluid after the FT reactor, the Grayson Streed method is used, which is recommended to simulate equilibria of a melt of hydrocarbons and hydrogen until a Temperature of 900 °F (482 °C) and a pressure below 3000 psia (207 bara) [15].

2.3. CO_2 capture unit

For this publication, we considered MEA process for carbon capture, as it is one of the most mature processes for this purpose. The thermal and electric demand is considered related to data of Roussanaly et al. [16] (thermal: 3.8 MJth/kgCO_2/Electricity: 0.45 MJel/kgCO_2). The desorption temperature is assumed to be at 120 °C for Pinch analysis [17].

2.4. SOEC

The Solid Oxide Electrolyzer Cell (SOEC) stands out as a cutting-edge electrolyzer technology, displaying promising results. It operates under elevated temperature conditions, which are essential for efficient electrolysis. As a result, the electrolysis in this case is applied on superheated steam instead of liquid water at approximately 800 °C. Consequently, the electric consumption is lower to produce the same amount of hydrogen compared to other low temperature technologies. The SOEC electrolyzer is based on a solid electrolyte composed from oxide ion conducting ceramics. The splitting of water molecule occurs in the cathode side, producing hydrogen molecules along with O^{2-} ions which are permeated to the anode through the membrane to be oxidized into oxygen molecules, according to the following reactions:

$$H_2O + 2\,e^- \rightarrow H_2 + O^{2-} \quad \text{Cathode}$$

$$O^{2-} \rightarrow \frac{1}{2}\,O_2 + 2e^- \quad \text{Anode}$$

SOEC seems to attract a lot of attentions lately, due to its very high overall efficiency and relatively low use of rare element compared to PEM. Nevertheless, its use is heavily dependent on the existence of heat synergies with nearby processes, considering the high heat consumption to evaporate water and heat up steam. The absence of such synergies will result in a low overall system efficiency (including electric and thermal efficiency). Fischer-Tropsch being an exothermic reaction, SOEC is an interesting electrolysis technology for this purpose [18] as heat integration between the processes will increase the overall energy

efficiency.

Electrochemical model: the polarisation curve of a SOEC shows the contribution of reversible and irreversible effects (ohmic losses, activation overpotential, concentration overpotential) [19].

$$U_{cell} = U_{rev} + \eta_{Ohm} + \eta_{MT,anode} + \eta_{MT,catode} + \eta_{act,anode} + \eta_{act,cathode}$$

The Fig. 2 shows a classic polarisation curve of a SOEC. There are 3 zones inside this curve:

- Activation overpotential zone (here before 0.2 A/cm^2), with a logarithmic behaviour
- Ohmic zone with a linear behaviour.
- Mass transfer limitation zone (here after 1.5 A/cm^2) with an exponential behaviour.

The different irreversible effects are difficult to dissociate, especially at stack or system level. Area Specific Resistance (ASR) is a useful tool for this purpose. The following equation gives the potential of the cell considering ASR:

$$U_{cell} = U_{rev} + ASR(T,t) \times j$$

The degradation of the cell leads to an increase of the ASR due to the effect of time on the performance of the cell. For this publication, a linear degradation is assumed, this means that evolution of ASR could be described by the following equation:

$$ASR(T,t) = ASR(T,t=0) \times (1 + t \times Deg)$$

With Deg the degradation rate.

The degradation rate is provided by considering the increase in voltage as a function of operating time, or as a function of the increase in ASR as a function of time. To standardise the results, if the degradation as a function of the ASR is not provided by the authors, then it is estimated using the increase of the voltage by the following formula:

$$Deg_{ASR} = Deg_V \times \frac{U_{tot}}{U_{irev}}$$

Table 1 presents in a non-exhaustive way, ASR and durability results at the stack level. For the energy analysis, values from Riedel et al. were chosen, in this publication the stacks have a low degradation over the period studied, moreover it has high performance for a stack composed of electrolyte supported cells. Finally, this stack is commercial. In order to compare an electrolyte-supported cell stack with a cathode-supported, values of Fang et al. and from Corre & Brisse were used. Jülich performance should be taken with precaution, as the stack is composed of only two cells, facilitating thermal management of the stack, the inlet flow has a H_2O/H_2 ratio equal to 1 potentially reducing the oxidation of the cell and increasing durability. Finally, this stack is not a commercial solution, therefore the result may not be reproducible.

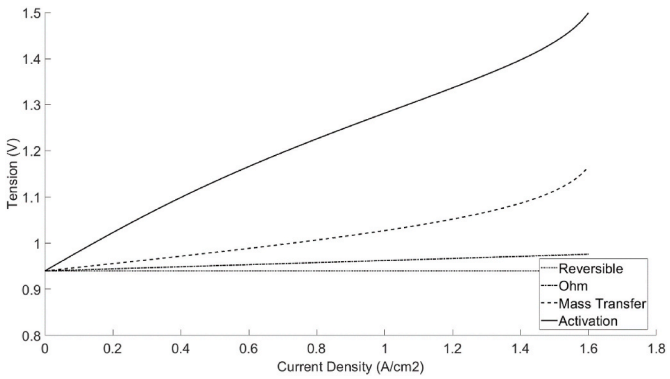

Fig. 2. Example of polarisation curve showing influence of Reversible, Activation Overpotential, Ohmic Resistance and Mass Transfer.

Table 1
Literature review of stack testing.

Article	Temperature (°C)	Ratio H_2/H_2O	Current density (A/cm^2)	Average cell voltage (V)	Steam utilisation (%)	Initial stack ASR (Ω.cm^2)	Degradation (% V/kh)	Degradation (% ASR/kh)	Test duration (h)	Cell active surface area (cm^2)	Number of cell in the stack	Fuel electrode or electrolyte supported	Date	Producer
Alenazey *et al.* [20]	750	90/10	1,1	1,3	70	0,422	n.a.	n.a.	n.a.	n.a.	6	Fuel electrode	2015	SOLIDPower
Corre & Brisse [21]	750	90/10	0,57	1,25	50	0,594	2.3	9.8	9000	87,7 (2192,5)	25	Cathode	2015	Haldor Topsoe
Fang *et al.* [22]	800	50/50	0,5	1,05	50	0,18	0.4	2.7	20000	80	2	Cathode	2018	Julich
Yan *et al.* [23]	800	50/50	0,5	1,05	50	0,217	15,82	197,38	990	80	4	Cathode	2017	Julich
Rinaldi *et al.* [24]	710–730	90/10	0,5	1,24	42	0,594	0,5	2.22	10700	48	6	Cathode	2017	SOLIDPower
Mougin *et al.* [25]	800	90/10	1,2	1,2	77	0,315	n.a.	n.a.	n.a.	100	25	Cathode	2017	CEA
Lang *et al.* [26]	820	80/9	0,52	1,29	70	1287	0,5	1.86	3370	128	30	Electrolyte	2019	Sunfire
Königshofer *et al.* [27]	830	80/ 20–95/ 5	0,78	1,4	80	0,721–0,811	n.a.	n.a.	n.a.	127,8	10	Electrolyte	2021	n.a.
Zheng *et al.* [28]	800	80/20	0,15	1,13	62	1635	11,7	74.04	1100	63	30	Cathode	2014	NIMTE
Sampathkumar *et al.* [29]	700	80/20	0,52	1,36	56	0,889	n.a.	n.a.	n.a.	100	5	Cathode	2022	DTU
Kusnezoff *et al.* [30]	800	80/21	0,4	1,2	75	0,53	n.a.	n.a.	n.a.	n.a.	10	Electrolyte	2021	IKTS
Hauch *et al.* [31]	700	90/10	1	1,16	95	0,286	n.a.	n.a.	n.a.	100	25	Cathode	2021	Elcogen
Riedel *et al.* [32]	800	90/10	0,5	1,4	70	1069	0.56	2.11	1000	127,8	10	Electrolyte	2019	Commercially available

However, the high performance of this stack gives an indication of what the future performance of fuel cell supported stack could be achieved in the near future. Values from Corre & Brisse are more representative of performance of a current cathode supported stack, the ASR is lower than that of an electrolyte supported, but on the other hand the degradation rate is higher.

Mass balance: this balance is driven by the two following equations:

$$F_{i,out} = F_{i,in} + \nu_i R_{elec}$$

$$R_{elec} = \frac{j}{2\ Far} \times A$$

With $F_{i,out}$, the molar flow of the species i (in mol/s), ν_i the stochiometric coefficient, R_{elec} the reaction rate in (mol/(s.m^2)), A the total area of the stacks in (m^2).

Energy balance: thermoneutral conditions are assumed. That means that the temperature at the exhaust of the system is equal to the temperature at the inlet of the stack. This hypothesis is quite acceptable, an SOEC is often operated near this condition to avoid mechanical stresses related to temperature gradient. Thermoneutral conditions assumed that the heat produced by the joule effect is compensated by the heat consumed by the endothermic splitting of H_2O. This energy balance is described by the following equation.

$$\dot{Q_{reac}} = \dot{Q_{Joule}}$$

With $\dot{Q_{reac}}$ the heat flux (in W) produced by the splitting of water and $\dot{Q_{Joule}}$ the heat flux produced by joule heating. These flux are defined as:

$$\dot{Q_{reac}} = \frac{jA}{2\ Far}\Delta h$$

$$\dot{Q_{Joule}} = j\ A\ U_{cell}$$

It is possible to determine $V_{thermoneutre}$, the voltage of the cell at thermoneutral conditions as

$$U_{thermoneutre} = \frac{\Delta h}{2.Far}$$

With Δh the specific enthalpy of the reaction at 800 °C, estimated at 248.3 kJ/mol with NIST database [14] corresponding to a thermoneutral voltage of 1287 V.

2.5. Reverse water gas shift and reformer

Reverse water gas shift is an equilibrium reaction between CO_2, H_2, CO and H_2O on a metallic catalyst. It transforms highly stable carbon dioxide molecule into carbon monoxide. The achievement of such result allows the Fischer-Tropsch downstream reactor to easily dissociate the carbon-oxygen bond in order to start the polymerization. Direct use of CO_2 in a Fischer-Tropsch reactor is not conventionally considered, since the existing F-T catalysts have low activity towards CO_2 dissociation. The rWGS reaction is slightly endothermic which means that a high temperature is needed to increase the reaction rate.

$$H_2 + CO_2 \leftrightarrow H_2O + CO \Delta H^0_{298} = 42kJ/mol$$

In the same reactional environment but under different operating conditions, other reactions can occur along with the targeted transformation. They mainly are:

➢ CO_2 direct hydrogenation to methane (Sabatier reaction)

$$CO_2 + 4H_2 \leftrightarrow CH_4 + 2H_2O \Delta H^0_{298} = -165kJ/mol$$

➢ Methanation reaction

$$CO + 3H_2 \leftrightarrow CH_4 + H_2O \Delta H^0_{298} = -206.5kJ/mol$$

Methanation and Sabatier reaction are very exothermic, as a consequence they are favoured at relatively low temperatures (between 300 and 400 °C). Keeping a fixed temperature at over 700 °C is mandatory for both high kinetics and avoidance of methanation/Sabatier reaction. To simulate this reactor, we consider an equilibrium reactor. This assumption is acceptable, generally for high temperature processes, products are near the thermodynamic compositions. The rWGS reactor operates at 900 °C and 4.1 bara.

Reforming is a very endothermic reaction. The objective of this reactor is to reduce the amount of methane and LPG turning around the process avoiding the use of a purge. The reactor transforms methane and LPG into syngas in order to recycle it into the Fischer-Tropsch reactor. The reaction below illustrates steam reforming of hydrocarbons:

$$C_nH_{2n+2} + nH_2O = nCO + (3n+1)H_2$$

In the model, reformer is modelled as a Gibbs reactor [33], the reformer operates at 900 °C and 1 bara. Reaction rate is defined related to CH_4 consumption.

For both reformer and rWGS reactor, heat to supply reactants at desired temperature is assumed to be supplied by the Heat Exchanger Network. The energy required to keep reactor at 900 °C is assumed to be supplied electrically, laboratory scale induction heated reformers currently perform with an efficiency of 23 % [34] to 50 % [35], but authors expect an efficiency of 90 % for an industrial scale process [34]. Because reformer and reverse water gas shift reactor are similar, for the simulation an efficiency of 90 % is assumed for both of them in all scenarios.

2.6. Fischer-Tropsch reactor

Fischer-Tropsch reaction is a hydrocarbon formation reaction. It is possible to split Fischer-Tropsch technologies into two, low temperature Fischer-Tropsch (LTFT) and high temperature Fischer-Tropsch (HTFT). The reaction follows different kinetics and yields different molecules in these two different cases. Fischer-Tropsch at high temperature gives shorter, more unsaturated molecules and more alcohols than Fischer-Tropsch at low temperature. Because the production of jet fuel requires the production of longer molecules without unsaturation, a LTFT is required for this work.

Fig. 3 shows the different reactor technologies for Fischer-Tropsch. Among the different technologies, two seem to provide the most interesting performances. Microchannel reactors are already used for Power to Liquid technology by INERATEC. However, they are not suitable for large scale production. Because of its high TRL, its high scalability and its high performance toward long chain hydrocarbon production, a slurry bed reactor is chosen for this study. A SBR is a reactor presenting three phases: a liquid phase, composed of liquid hydrocarbons, solid catalysts are in suspension into this liquid phase. The gaseous reactants are distributed at the bottom fluidizing the slurry. This kind of reactors has a conversion rate, related to CO, of maximum 60–65 % [36].

➢ Hydrodynamic of the FT reactor

To size the Slurry reactor and to assure the possibility of conversion rate related to operating conditions. The column is modelled according to the publication proposed by Maretto and Krishna [37]. In order to validate the hydrodynamics, the authors used several studies conducted by the University of Amsterdam on pilot scale reactors (ranging from 0.1 to 0.63 m in diameter and 1.2–4 m in height) [38–42]. The size of the equipment used to validate the model, along with the quality of the fitting, give confidence in the hydrodynamics. The assumptions of the model are:

- Churn regime ($V_G \in [0.1, 0.5]$ m/s and $V_L \approx 0.1$ m/s)

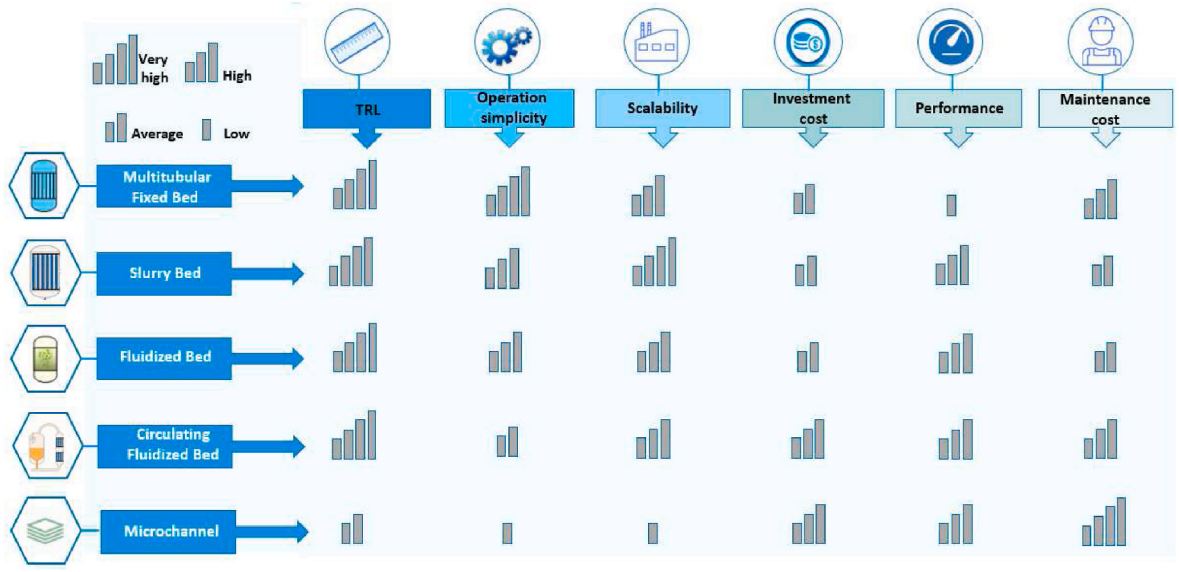

Fig. 3. Fischer-Tropsch reactors technologies evaluation.

- Isotherm condition is achieved as a consequence of the Churn-turbulent regime.
- Gas flow is separated into two different phases, a large bubble phase with a plug flow. And a small bubble phase considered into a perfectly stirred phase.
- The liquid phase is considered perfectly stirred.
- Solid catalyst is in suspension homogenously in the liquid phase.
- Solid concentration is higher than 0.16 and lower than 0.38, all the bubbles are considered virtually destroyed at higher solid concentration.

For a slurry bed reactor, a Churn turbulent regime, the gas holdup is defined as the sum of the hold up of large bubble (ϵ_{LB}) and small bubble (ϵ_{SB}) in the reactor:

$$\epsilon = \epsilon_{LB} + \epsilon_{SB}(1 - \epsilon_{LB})$$

In the simulation, the large bubble is affected by the syngas conversion proportionally to the syngas conversion. But the small bubble holdup is considered constant all along the reactor. This holdup is determined with the equations below:

$$\epsilon_{SB} = \epsilon_{SB,ref}\left(1 - \frac{0.7}{\epsilon_{SB,ref}}\epsilon_S\right)\left(\frac{\rho_G}{\rho_{G,ref}}\right)^{0.48}$$

The small bubble velocity, $U_{G,SB}$ (m/s), is estimated using the following formula:

$$V_{G,SB} = \epsilon_{SB} V_{small}$$

With V_{small} the rise velocity of small gas bubbles which is also influenced by the solid holdup in the slurry reactor. This velocity can be calculated with this correlation developed by Krishna et al. [40]

$$V_{small} = V_{small,ref}\left(1 + \frac{0.8}{V_{small,ref}}.\epsilon_S\right)$$

The large gas bubble holdup can be estimated using the following correlation:

$$\epsilon_{LB} = 0.3\frac{1}{V_{G,LB}^{0.22}}(V_{G,LB})^{4/5}$$

The volumetric mass transfer coefficient for large and small bubbles are estimated as follows:

$$(k_L a)_{LB} = 0.5\sqrt{\frac{D_{L,i}}{D_{L,ref}}}\epsilon_{LB}$$

$$(k_L a)_{SB} = 1.0\sqrt{\frac{D_{L,i}}{D_{L,ref}}}\epsilon_{SB}$$

Large gas bubbles are assumed to be in the plug flow manner:

$$\frac{dC_{Gi,LB}}{dz} = -(k_L a)_{LB}\left(\frac{C_{Gi,LB}}{m_i} - C_{Li}\right)\frac{1}{V_{G,LB}}$$

$$z = 0 \;;\; C_{Gi,LB} = C_G^{in} i, LB$$

With $C_{Gi,LB}$ and C_{Li} correspond to the concentration of constituent i in the large bubbles and the liquid phase respectively (mol/m^3). m_i is the partition coefficient or the solubilities of constituent i, which is by definition: $m_i = C_G/C_L^*$..

The velocity of the large bubble, $U_{G,LB}$ evolves along the reactor and decreases with conversion:

$$V_{G,LB} = V_{G,LB}^0(1 + \beta.X_{CO})$$

$$X_{CO} = \frac{F_{G_{CO}}^{in} - F_{G,LB_{CO}}^{out} - F_{G,SB_{CO}}^{out} - F_{L_{CO}}^{out}}{F_{G_{CO}}^{in}}$$

Assuming that the small gas bubble phase is well-mixed:

$$\left(C_{G_{i,SB}}^{in} - C_{Gi,SB}\right) = (k_L a)_{SB}\left(\frac{C_{Gi,SB}}{m_i} - C_{Li}\right)\frac{H}{V_{G,SB}}$$

Where it is assumed that the initial concentration of syngas in the small bubble is equal to the syngas concentration in the large bubbles at the inlet of the reactor. The velocity of the small bubbles is assumedly constant and not influenced by the syngas conversion unlike the velocity of the large gas bubbles.

The mass balance inside the liquid phase gives:

$$(C_{L_i}^E - C_{L_i}) + \int_O^H (k_L a)_{LB}\left(\frac{C_{Gi,LB}}{m_i} - C_{Li}\right)dz\frac{1}{V_L} + (k_L a)_{SB}\left(\frac{C_{Gi,SB}}{m_i} - C_{Li}\right)\frac{H}{V_L} = \frac{\varepsilon_S \varepsilon_L \rho_s H}{V_L}\nu_i r_{FT}$$

With U_L the slurry phase velocity (m/s), ρ_S is the density of the slurry phase (kg/m^3) and r_{FT} is the rate of Fischer-Tropsch reaction kinetics (mol/kg$_{cat}$.s). Meanwhile, ϵ_L corresponds to the liquid holdup and equates to $(1-\epsilon_G)$. The parameters used in the calculation are summarized in Table 1 in the supplementary material

➢ Kinetic

The kinetics used come from Yates and Satterfield [43], with modified parameters from Maretto and Krishna [37] fitted with experimental data from Refs. [38–42], which derived from a Langmuir Hinshelwood model:

$$r_{CO} = \frac{a\, C_{L,CO} C_{L,H2}}{\left(1 + bC_{L,CO}\right)^2}$$

With a being the reaction rate and b being the adsorption constant, calculated by (parameters used are summarized in Table 2 in SI)

$$a = a_0 \exp\left(\frac{-Ea}{R} \times \left(\frac{1}{493.15} - \frac{1}{T}\right)\right) \times (R\,T)^2$$

$$b = b_0 \exp\left(\frac{\Delta Hb}{R} \times \left(\frac{1}{493.15} - \frac{1}{T}\right)\right) \times (R\,T)$$

➢ Product distribution

In case of ASF distribution, the molar fraction of product with carbon number of i is:

$$x_i = (1-\alpha)\alpha^{i-1}$$

And α is defined as:

$$\alpha = \frac{r_P}{r_P + r_T}$$

With r_P, the rate of propagation and r_T the rate of termination. This distribution allows to have a quick estimation of the exhaust product. The Fig. 4 shows the product distribution related to α considering no deviation.

Deviations occur not only for heavier molecules. Experimental results show four different deviations for Fischer-Tropsch products distribution. Several experiments suggest that deviations from ASF distribution can occur especially for:

- Methane production (C1), with a higher selectivity
- Ethane production (C2), with a lower selectivity
- Heavy hydrocarbon production (C10+), with a higher selectivity

To estimate α as a function of the operating conditions of the reactor, the product distribution proposed by Vervloet is used [44]:

$$\alpha = \frac{1}{1 + k_\alpha \left(\frac{P_{H_2}}{P_{CO}}\right)^{\beta} exp\left(\frac{\Delta E_\alpha}{R}\left(\frac{1}{493.15} - \frac{1}{T}\right)\right)}$$

Table 2
Mass balance of the base case.

Product	Base Case
Outlet	
Jet-Fuel (ton/h)	8.76
Naphtha (ton/h)	1.91
Oxygen (ton/h)	37.22
Inlet	
Water for electrolysis (ton/h)	14.84
CO_2 (ton/h)	33.14

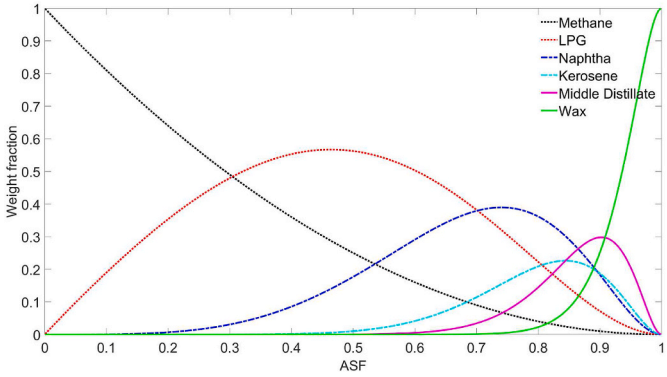

Fig. 4. Product distribution related to ASF distribution.

The ASF selectivity was fitted by the authors of this publication using data from various sources with different Co catalysts (both promoted and unpromoted, and with different supports). The data was collected for temperatures ranging between 450 and 530 K and H2/CO ratios ranging between 1 and 3.

Methane and ethane deviations are estimated by specific reaction rate coming from the publication of Pandey et al. [45]. Parameters used are summarized in Table 3 in SI.

$$r_{CH_4} = k_{CH_4}\, r_{CH_4,ideal}\, p_{H_2}$$

$$r_{C_2H_6} = k_{C_2H_6}\, r_{C_2H_6,ideal}$$

The value from Pandey was checked against values from various sources found in the literature [38,41–54]. Parity plots of methane selectivity and C2C4 selectivity can be found in Figs. 1 and 2 in the SI. It is assumed that C3 and C4 follow the ASF distribution. The fit to the experimental data is rather poor, especially for methane selectivity, but the model can provide an estimate of methane production for a wide range of process conditions and catalysts.

2.7. Pre-separation and distillation

The objective of this unit of this process unit (reported in Fig. 5) is to separate unreacted syngas, light gases and water from FT liquid products. To allow this separation, the decrease in temperature and pressure is sequenced between the operating conditions of the Fischer-Tropsch reactor (220–240 °C and 20 bara) and the operating condition of the distillation column (100 °C and 2,5 bara). For the gas side, the pressure only decreases to 18 bara, in order to reduce the compression cost required to recycle the unconverted syngas in the reactor. The

Table 3
Energy balance of the base case.

Energy balance	Base Case
Outlet	
LHV of product (MW)	127.80
LHV Jet-Fuel (MW)	104.79
LHV Naphtha (MW)	23.01
Low quality heat (<100 °C) (MW)	17.41
Inlet	
Total Electric Need (MW)	271.30
Heat need (MW) (% total)	0.54 (0.20 %)
SOEC Electric demand (MW) (% total)	200.0 (73.88 %)
Electric need for Carbon Capture (MW) (% total)	6.36 (2.35 %)
Compressors and pumps (MW) (% total)	23.72 (8.76 %)
Distillation (MW) (% total)	8.32 (3.07 %)
Electric need for rWGS (MW) (% total)	7.71 (2.85 %)
Electric need for Reformer (MW) (% total)	24.07 (8.89 %)
Efficiency	
Power to Liquid efficiency (%)	47.21
Power to Jet-Fuel efficiency (%)	38.71

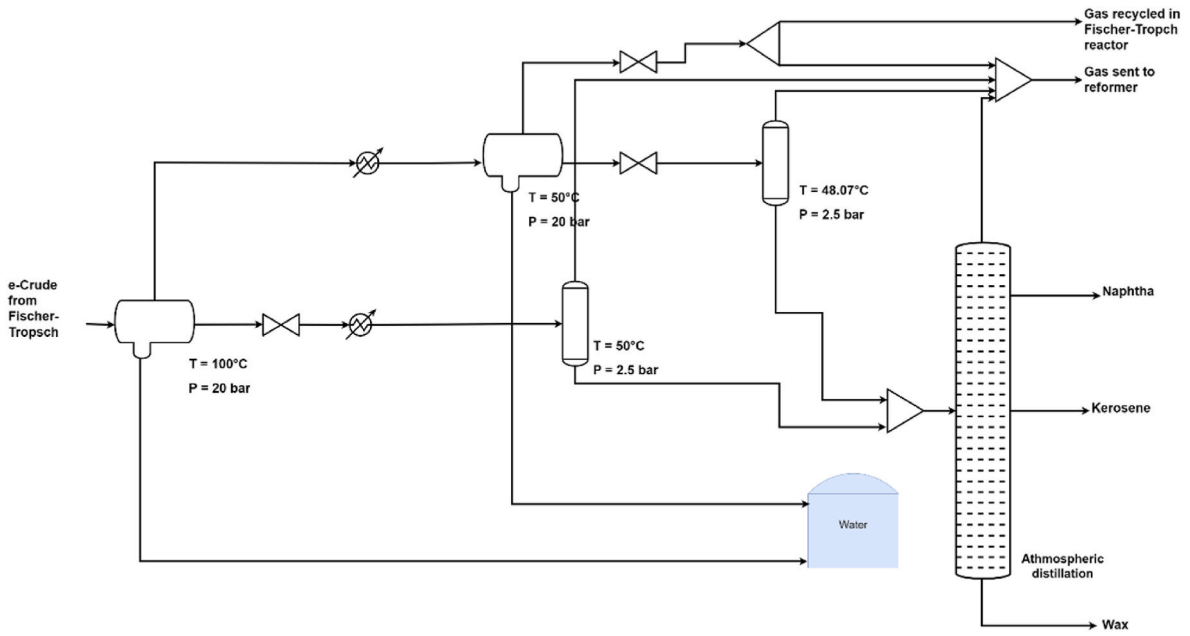

Fig. 5. Process diagram of the pre-separation unit and the distillation section.

separation is carried out in three-phase flash separator units or two-phase flash separators (in this case there are only two exhausts for oil and gas).

The water is separated due to its immiscibility with oil, and it is recycled back into the high temperature electrolyser. The gas from the distillation column and from the pre-separation is rich in unconverted syngas, methane and LPG. Gas collected from pre-separation is divided into two streams, one of which is directly returned to the Fischer-Tropsch reactor. The other portion is sent to the reformer with the off-gases from the distillation column. To reach specification for jet-fuel. Liquid hydrocarbons must be sent to a stricter separation unit using a fractional distillation column based on the difference of volatility between the different components:

- Remaining gases are recovered from the top along with remaining water which condensates in the condenser
- Gasoline is recovered then
- Kerosene is recovered from the middle
- Diesel and waxes are sent to the bottom

Distillation is a heat consuming unit, in this publication heat is assumed to be supplied electrically. A consumption of 440 MJth/ton is assumed [46]. Synthetic crude is lighter than conventional crude, so a lower consumption could be expected.

The gas taken from the three-phase separator at 50 °C is rich in unreacted syngas and in light gases, the splitting ratio between gas sent directly in the Fischer-Tropsch reactor and the gas sent to the reformer is set to 50 % in Base Case.

The composition of the oil fractions out of the distillation section is calculated with the ECP (extended cutting plane). This method is a solution to approximate the MINLP problem of the Liquid Vapor equilibrium of a multicomponent fluid at different temperature. For the simulation, an isobar distillation is assumed. Typical atmospheric distillation section mainly operates from 0.5 barg to 2 barg [47]. In the simulation a pressure of 2.5 bara is chosen (1.5 barg). The parameters used in the calculation are summarized in Table 4 in the supplementary material.

Table 4
Accordance between Power-to-Liquid jet fuel and regulation.

Properties		ATSM regulation for FT SPK	Result of simulation (Base Case)
10 % recovered temperature (T10) (°C)	Max	205	162.7
Final Boiling Point (°C)	Max	300	297.4
T90-T10 (°C)	Min	22	111.4
Flash Point (°C)	Min	38	41.11
Density at 15 °C (kg/m^3)	Min-Max	730–770	750.3
Freezing point (°C)	Max	−40	−61.72
Cycloparaffins (%)	Max	15	0
Aromatics (%)	Max	0.5	0

2.8. Hydrocracking

This technology of cracking aims at producing lighter fractions with higher jet fuel and diesel productivities. In a general use in refineries, and considering the high sulphur and impurity content, this unit is composed of two reactors, the first one is called hydrotreatment reactor and is mandatory to remove all the metallic impurities, sulphur, aromatics, olefins and especially components with nitrogen, while the second reactor is only for hydrocracking reactions. To crack Fischer-Tropsch waxes, it is assumed that no impurities are present, thereby necessitating the use of only one reactor [48–50]. The Fig. 6 presents the simplified diagram of a typical hydrocracker with two reactors. The reaction below shows an example of hydrocracking reaction.

$$C_{20}H_{42} + H_2 \rightarrow C_{12}H_{26} + C_8H_{18} \left(\Delta H^0_{298} = -45 \text{ to } -53 \text{ kJ} \,/\, \text{mol } H_2\right)$$

In a normal operation of a HCC, both reactors are operating under a very high pressure of between 100 and 170 bara depending on the nature of feedstock, and a temperature of about 400 °C. For the purpose of cracking Fischer-Tropsch waxes and diesel cut in order to increase jet fuel selectivity, milder operating conditions could be applied. Cracking of hydrocarbons in the reactor is simulated based on the model from Gambaro et al. [51] with modified kinetics from Sun et al. [52]. This model used different assumptions:

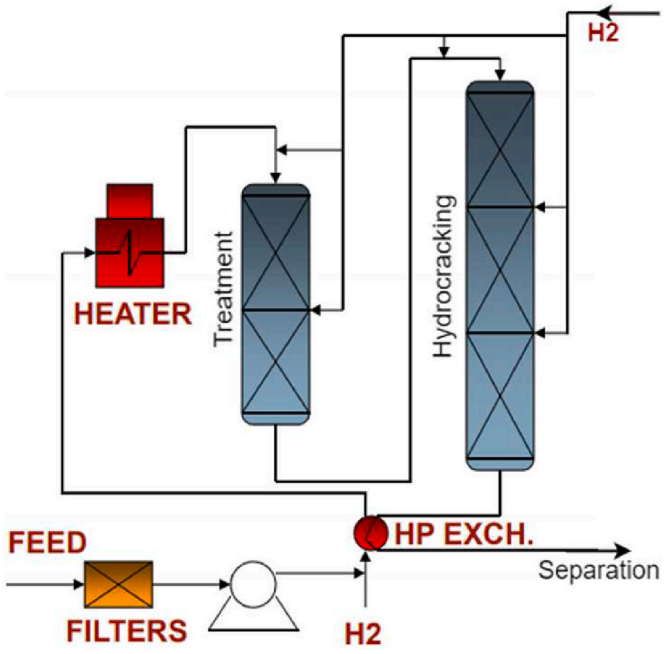

Fig. 6. Schematic representation of a hydrocracking unit.

- Iso-C5 could not crack, because its cracking is assumed to produce a primary carbenium ion (CH_3^+)
- Only isoparaffins from C6 to C75 are cracked
- Iso-C6 are the only molecules that lead to the production of methane and ethane
- Cracking can lead to the production of both n-paraffin and isoparaffins
- The cracking probability prioritizes the cracking of the middle bond and forbids the cracking of the last or first C–C bonds.
- All iso-paraffin of a same carbon number are represented by a pseudo-component named iso-paraffin

The kinetics scheme is led by isomerisation, cracking and formation of molecules from cracking [52]. The kinetic scheme of the reaction presented below derived from a Langmuir-Hinshelwood approach.

$$R_{iso,i} = \frac{k_{iso,i}\left(c_{n,i} - \frac{c_{iso,i}}{K_{eq,i}}\right)}{ADS}$$

$$R_{cr,i} = \frac{k_{cr,i} c_{iso,i}}{ADS}$$

$$R_{form,iso,i} = 0.903 \sum_{j=i+4}^{75} \left(2 \times \frac{R_{cr,j}}{j-6}\right) + \frac{R_{cr,(i+3)}}{j-3} \quad (i = 4-71)$$

$$R_{form,iso,47} = \frac{R_{cr,50}}{i-3}$$

$$R_{form,n,i} = 0.097 \sum_{j=i+4}^{75} \left(2 \times \frac{R_{cr,j}}{j-6}\right) \quad (i = 4-71)$$

$$R_{form,3} = \sum_{j=7}^{75} \frac{R_{cr,j}}{j-6}$$

$$ADS = c_{H_2}\left(1 + \sum_{1}^{75} c_{n,i} K_{n,i} + \sum_{4}^{75} c_{iso,i} K_{iso,i}\right)$$

$$k = k^0 \exp\left(\frac{-Ea}{R} \times \left(\frac{1}{T} - \frac{1}{T_{ref,HCC}}\right)\right)$$

The reactor is modelled as a plug flow reactor. In the model, 148 components are considered, their mass balances are defined in the equations below.

$$r_{iso,i} = R_{iso,i} + R_{form,iso,i} - R_{cr,i} \quad i \geq 6$$

$$r_{iso,5} = R_{iso,5} + R_{form,iso,5}$$

$$r_{iso,4} = R_{form,iso,4}$$

$$r_{n,i} = -R_{iso,i} + R_{form,n,i} \quad i \geq 6$$

$$r_{n,5} = -R_{iso,5} + R_{form,n,5} + 0.4\, R_{cr,6}$$

$$r_{n,i} = R_{form,n,i} + 0.4\, R_{cr,6} \quad i = 3,4$$

$$r_i = 0.4\, R_{cr,6} \quad i = 1,2$$

$$r_{H_2} = \sum_{6}^{75} R_{cr,i}$$

The operating range of the Sun/Gambaro model is T = 225–255 °C, WHSV = 6–12, P = 30 bara, H_2/wax = 0.06–0.15 g/g [51,52]. However, experiments carried out by Sun et al. in order to fit kinetics parameters were realised with a lab scale test reactor, the bed contains 1 g of catalyst and the catalyst bed is 1.5 mm thick. So it should be kept in mind that these kinetics could be not relevant for an industrial size reactor. Kinetics parameters are considered with the following equation and the value reported in the Table 6 in SI:

$$k^0_{iso,i} = k^0_{iso,i}, m \times i^{k^0_{iso,i},n}$$

$$k^0_{cr,i} = k^0_{cr,i}, m \times i^{k^0_{cr,i},n}$$

$$E^0_{iso,i} = E^0_{iso,i}, m \times i^{E^0_{iso,i},n}$$

$$E^0_{cr,i} = E^0_{cr,i}, m \times i^{E^0_{cr,i},n}$$

It is assumed that only condensed molecules could react and so a Liquid-Vapor equilibrium is computed according to the Raoult Law:

$$K_i = \frac{y_i}{x_i} = \frac{P_i^{vap}}{P}$$

Molecules lighter than C5 (including C5) are typically found exclusively in the vapor phase. This estimation poses no issues since, based on the assumptions of the models, molecules lighter than C5 are not expected to undergo cracking. For molecules heavier than C6 (included) vapor pressure is estimated from Marano and Holder correlation [53].

$$P_i^{vap} = \exp\left(2.72709 + A\,(i - 1.126231) - B \exp\left(\right.\right.$$
$$\left.\left. - 0.619226(i - 1.126231)^{0.416321}\right)\right)$$

$$A = 15.8059 - \frac{1496.56}{T} - 2.17342 \log(T) + 7.27763 \,.\, 10^{-7} T^2 + \frac{37876.2}{T^2}$$

$$B = -5.75509 - \frac{7.56568}{T} + 0.0857734 \log(T) - 1.41964 \,.\, 10^{-5} T^2 + \frac{267209}{T^2}$$

The purpose of the separator after the hydrocracker is twofold. The first objective is to recover as much hydrogen as possible to reduce hydrogen consumption, and to recover the liquid fraction in order to send it to the distillation fraction. The gas recovered from pre-separation

is rich in hydrogen, but could contain light gases such as methane, also a purge is required. In this study, the splitting rate is fixed for all simulations, 99.8 % of gases is sent back to the hydrocracking reactor. The Fig. 7 shows a schematic representation of the pre-separation and the distillation following the hydrocracker.

The operating conditions of this column are slightly different than the one of the first column, because the hydrocarbons mixture that comes inside is heavier and so the temperature between kerosene and wax fraction has to be higher to respect ASTM specifications. Parameters used for this distillation column are presented in Table 5 in SI.

2.9. ASTM

ASTM is a United States government organization responsible for the standard for aviation fuels. Other organizations offer standards for aviation fuel, such as GOST 10227, valid in CIS countries, or GB 6537 in China, but none of them are as important as ASTM D1655 which specifies Jet-A and Jet-A1 fuels, valid worldwide. The ASTM specifications are the only ones presented in this article due to their ability to be used worldwide. ASTM D7566 allows the use of Alternative Aviation Fuel, such as Fischer-Tropsch Jet-fuel. If an Alternative Aviation Fuel, from a process allowed by this regulation meets the requirement, it could be used, mixed with conventional jet fuel, in civil aviation.

The fuels have many fit-to-purpose properties such as thermal coefficient, surface tension, specific heat, enthalpy of evaporation, dielectric constant, electrical conductivity, flammability limits with altitude, minimum spark ignition energy, spontaneous ignition, bulk modulus solubility of gases and water, thermal oxidation stability. Table 7 in SI gives the values from ASTM D7566 that are limiting for the process.

3. Results and discussion

In this section, the results of the simulation are presented. In the first part, the results of a baseline scenario are presented in a comprehensive manner. In the second part, the influence of the three most important bricks of the process is analysed in detail. Then, an ANOVA analysis is performed to analyse the influence of process parameters, as well as their interactions on the overall efficiency of the process as well as its selectivity. Finally, a comparison with other results from the literature will be presented. The performance of the process is analysed with two indicators, Power to Liquid efficiency, defined as:

$$PtL_{efficiency} = \frac{\dot{M}_{products} \times LHV_{products}}{Electric\ consumption}$$

and kerosene selectivity defined as:

$$Selectivity = \frac{\dot{M}_{kerosene}}{\dot{M}_{products}}$$

Table 5
Energetic comparison between No-Naphtha scenario and Base Case.

Energy balance	Base Case	No Naphtha
Outlet		
LHV of product (MW)	127.80	127.04
LHV Jet-Fuel (MW)	104.79	127.04
LHV Naphtha (MW)	23.01	0.0
Low quality heat (<100 °C) (MW)	17.41	47.41
Inlet		
Total Electric Need (MW)	271.30	290.51
Heat need (MW) (% total)	0.54 (0.20 %)	1.23 (0.42 %)
SOEC Electric demand (MW) (% total)	200.0 (73.88 %)	200.0 (68.85 %)
Electric need for Carbon Capture (MW) (% total)	6.36 (2.35 %)	6.37 (2.19 %)
Compressors and pumps (MW) (% total)	23.72 (8.76 %)	27.98 (9.63 %)
Distillation (MW) (% total)	8.32 (3.07 %)	9.97 (3.43 %)
Electric need for rWGS (MW) (% total)	7.71 (2.85 %)	7.72 (2.66 %)
Electric need for Reformer (MW) (% total)	24.07 (8.89 %)	33.52 (12.82 %)
Efficiency		
Power to Liquid efficiency (%)	47.21	43.73
Power to Jet-Fuel efficiency (%)	38.71	43.73

3.1. Base case

The parameters used for the base case scenario are:

- CO conversion in the Fischer-Tropsch reactor: 50 %

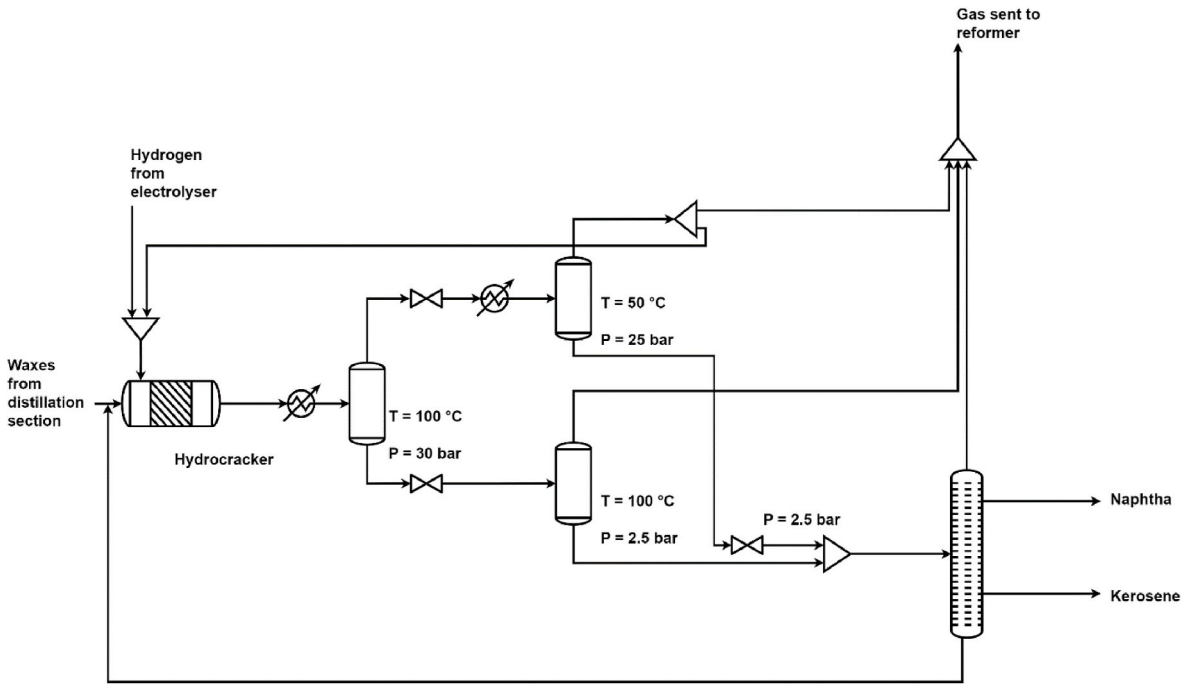

Fig. 7. Process diagram of the distillation section and separation.

Table 6
Influence of replacement rate on mean efficiency of the plant.

Considering operating parameters from publications						
	ESC (Commercially available - Fang et al.)		CSC (Jülich – Riedel et al.)		CSC (Haldor-Topsoe – Corre & Brisse)	
	Mean Power consumption (MW)	Global efficiency (%)	Mean Power consumption (MW)	Global efficiency (%)	Mean Power consumption (MW)	Global efficiency (%)
Initial	181.0	51.09	132.1	61.85	149.3	54.75
1 year	186.2	50.05	133.3	61.49	162.8	51.74
4 years	201.9	47.15	136.7	60.49	203.3	44.41
10 years	233.4	42.24	143.7	58.54	284.3	34.60
Considering same operating parameters						
	ESC (Commercially available - Fang et al.)		CSC (Julich – Riedel et al.)		CSC (Haldor-Topsoe – Corre & Brisse)	
	Mean Power consumption (MW)	Global efficiency (%)	Mean Power consumption (MW)	Global efficiency (%)	Mean Power consumption (MW)	Global efficiency (%)
Initial	179.1	51.16	123.7	65.73	149.4	58.06
1 year	184.3	50.11	124.8	65.36	169.4	54.22
4 years	200.0	47.21	128.2	64.25	205.5	46.26
10 years	231.4	42.30	134.9	62.15	306.6	35.78

Table 7
Comparison of the current density on the required number of stack and efficiency.

		ESC (Fang et al.)	CSC (Julich)	CSC (Haldor-Topsoe)
0.5 A/cm²	**Area (m²)**	24 933 m²		
	Stack x cell	194 790 Stacks x 10 cells (128 cm²)	1 558 300 Stacks x 2 Cells (80 cm²)	113 330 Stacks x 25 cells (88 cm²)
	PtL efficiency (%)	47.21	64.25	44.71
0.75 A/cm²	**Area (m²)**	16 622 m²		
	Stack x cell	129 860 Stacks x 10 cells (128 cm²)	1 038 900 Stacks x 2 Cells (80 cm²)	75 555 Stacks x 25 cells (88 cm²)
	PtL efficiency (%)	40.61	61.73	39.72
1.00 A/cm²	**Area (m²)**	12 467 m²		
	Stack x cell	97 396 Stacks x 10 cells (128 cm²)	779 170 Stacks x 2 Cells (80 cm²)	56 667 Stacks x 25 cells (88 cm²)
	PtL efficiency (%)	35.67	57.15	34.80

- H_2/CO ratio at the inlet: 2
- Methane conversion in the reformer: 50 %
- Temperature of the Fischer-Tropsch reactor: 220 °C
- Direct recycling rate: 50 %
- Temperature of the hydrocracker: 242 °C

3.1.1. Mass and energy balance

Due to the choice not to use a burner to recover waste gases, the carbon yield is equal to 100 %. There is no other exhaust for carbon different from naphtha or jet-fuel. The large amount of oxygen, produced in the form of oxygen enriched air, is difficult to value. All the water produced is sent back to the electrolyser. Indeed, the simulation does not show the quantity of hydrocarbons in the water produced from the Fischer-Tropsch reactor because of the thermodynamic model. The chosen equation of state makes it possible to obtain good estimates of the Liquid-Vapor equilibrium in the presence of hydrogen, to the detriment of the quality of the prediction of the Liquid-Liquid equilibriums. In reality a small amount is expected to be in the water and has to be treated before being released to the environment. But in the case of a SOEC for hydrogen production, it is assumed that a small amount of hydrocarbons could be reformed inside the SOEC without impacting the system. The Table 2 presents the mass balance of the base case.

To calculate the energy content in energy balance, presented in the Table 3, a LHV of 12 MWh/ton is assumed for liquid product. The process produced 17.41 MW of low-quality heat, that is difficult to valorise, but harnessing that heat could greatly benefit system efficiency. The main energy consuming part of the process is the electrolyser, 73.88 % of the electric demand is consumed by the SOEC for H_2 production. The second main consuming element of the process is the reformer which consumes 8.89 % of the global electric demand. Compressors and pumps have a similar energetic cost consuming 8.76 % of total required electricity, compressors are estimated with an adiabatic efficiency of 75 %. Excluding Naphtha production, power to jet fuel efficiency is around 38.71 %.

Fig. 8 shows the Pinch analysis (with $DT_{min} = 10$ °C) of the process. Almost all the heat consumed is produced by the process, which allows us to use only 0.54 MW of electricity for heating. The heat consumed in the rWGS and in the reformer which is considered apart and so excluded from the composite curve. The hot composite curve is composed of the cooling of the exhaust gas from the SOEC, rWGS and reformer between

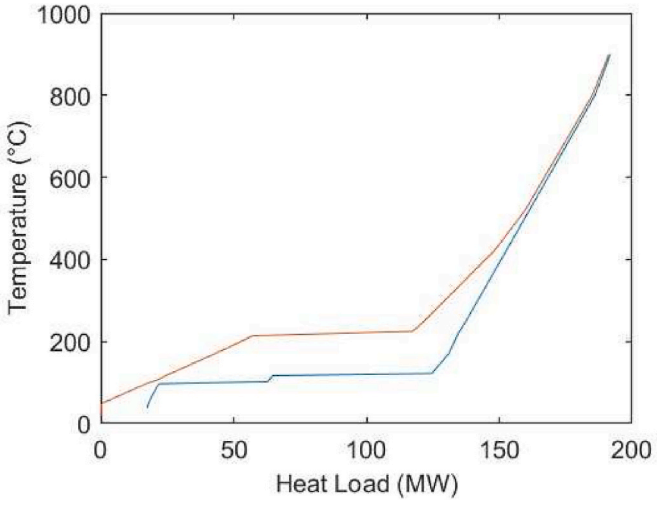

Fig. 8. Hot and cold composite curve of Power-to-Jet-Fuel process in Base Case scenario.

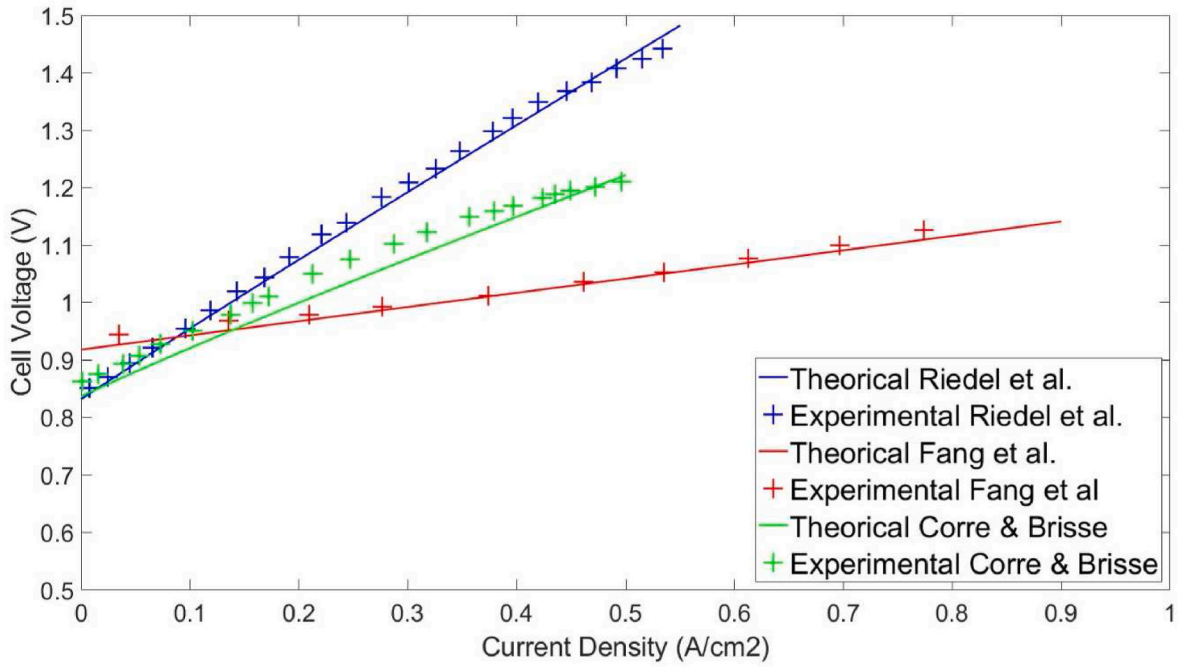

Fig. 9. Comparison between experimental and theoretical polarisation curve with data from Riedel et al. Values obtained with a conversion rate of 0.6 for j = 0.8 A/cm^2, $PH_2O/PH_2 = 9$, T = 800 °C, $P_{tot} = 1.4$ bara, air electrode is supplied with air with a ratio $Flow_{air}/Flow_{fuel} = 10$. Fang et al. Values obtained with a conversion rate of 1 for j = 1.0 A/cm^2, $PH_2O/PH_2 = 1$, T = 800 °C, $P_{tot} = 1.0$ bara, air electrode is supplied with air with a ratio $Flow_{air}/Flow_{fuel} = 8$ after 500 h of operation Corre & Brisse. Values from cells from group 4 obtained with a conversion rate of 0.50 for j = 0.50 A/cm^2, $PH_2O/PH_2 = 9$, T = 750 °C, $P_{tot} = 1.0$ bara, air electrode is assumed to be supplied with air with a ratio $Flow_{air}/Flow_{fuel} = 1$.

900 °C and 220 °C. At this temperature, a plateau is observed, representing the heat produced by the Fischer-Tropsch reactor. In a last part, there is the cooling of the different products of the reactor from 220 °C to 20 °C.

The cold composite curve is composed of the heating of water from 20 °C to 100 °C in a first part. There is a first plateau representing the heat required to vaporize the water at 100 °C. Then, there are a second plateau representing the heat consumed by the regeneration of MEA in the process at 120 °C. Then, in a last part, there is the heating of the gas to supply either the reformer, the rWGS or the SOEC.

3.1.2. *Final product distribution and comparison with ASTM regulation*

Fig. 3 in SI shows the mass distribution in naphtha and kerosene fraction. The kerosene fraction is mainly composed of molecules with a carbon number between C8 and C17. The naphtha fraction is mainly composed of molecules between C5 and C8. The molecules produced by the FT reactor having a lower carbon number were sent to the reformer. Molecules heavier than C17 were sent to the hydrocracking reactor to be cracked there and thus improve the selectivity towards these two fractions. Table 4 presents the compliance between Power to Liquid jet-fuel and ASTM regulation. The values for cycloparaffins and aromatics are 0 due to the choice to use a modified ASF for product distribution. The model is therefore not able to estimate the production of these molecules. But it is known that the amount of aromatics produced in an LTFT is trace, less than 0.1 % [54].

The proximity between the flash point of the final product and the minimum authorised by the ASTM does not allow the introduction of lighter molecules without the risk of falling below this limit. Similarly, the proximity between the final boiling point and the maximum authorised does not allow the introduction of heavier molecules. It is therefore not possible to improve the selectivity by modifying the operating conditions of the distillation columns.

3.1.3. *Influence of naphtha production on efficiency*

The production of naphtha is mainly intended for the petrochemical industry in order to enable its decarbonation. As a fuel, the naphtha produced has characteristics that make it difficult to bring it to market. In the event that no market could absorb the production of e-naphtha, this product could be recycled in the reformer with LPGs, the Table 5 gives the energy efficiency of the Power-to-liquid process whose only output product would be jet fuel compared to the base case.

A significant drop in overall energy efficiency is observed by recycling the naphtha within the reformer. Moreover, this simulation does not take into account the significant risk of carbon deposition in the context of naphtha steam reforming, the deposit of carbon leads to a loss of material, in the solid carbon, additional costs related to the regeneration of the catalyst should be expected.

3.2. *Analysis of main process elements*

3.2.1. *Influence of solid oxide cell technology*

Fig. 10 a, b, c show the comparison between the simplification of a cell operation using ASR and the experimental results from the

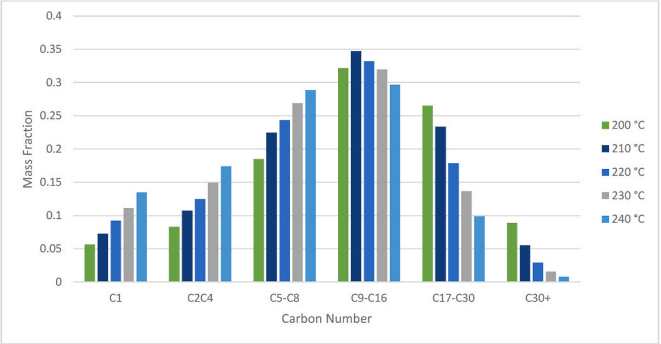

Fig. 10. Mass repartition of Hydrocarbons out of Fischer-Tropsch reactor relative to the temperature.

literature. The effectiveness of linearizing irreversibilities can be observed in accurately predicting cell operations at low current densities. For graphs a and c, a less linear behaviour is experimentally observed around 0.4 A/cm^2.

Cathode supported cells for electrolysis are less developed than electrolyte-supported cells. This technology offers better performance but generally the degradation rate is too high to allow the use of this technology to produce a large quantity of H_2. Therefore, the ASR values and degradation rate of Fang et al. should be taken with caution, the stack used consisted of only 2 cells. It is easier to manage heat in a small unit than in a larger one. Moreover, this stack is not commercially available, and it is important to see if these results are repeatable in a larger unit. However, the development and use of cathode-supported cells could have a huge impact on efficiency. To allow a comparison with an industrially produced cathode-supported stack, a comparison was made with the Corre & Brisse study. This stack has a lower initial ASR than the Fang et al. stack, but the degradation is faster as expected with this technology.

➢ Comparison between cell technology on efficiency of the process

Table 6 shows the influence of cell technology on the overall process efficiency. The stacks operate under the operating conditions under which they were tested. The CSCs stacks show a higher initial efficiency than the ESCs. However, on the stack proposed by Haldor Topsoe, the degradation is significant. The CSC stack from Corre & Brisse is less efficient than the ESC from Riedel et al. after 4 years and 85 % of load rate. Based on the initial characteristics, it becomes apparent that the Haldor Topsoe stack exhibits superior energy efficiency compared to the electrolyte-supported stack, despite operating at a temperature of 750 °C. The Jülich stack performs much better than the other stacks, both in terms of efficiency and durability. This stack may serve as a clue to what commercial cathode-supported cell stacks may offer in the future.

The part "Considering operating parameters from publication" of the Table 6 compares the different stacks under different operating conditions, making it impossible to discern the variation in efficiency due to the operating conditions or to the stack itself. Part. "Considering same operating parameters" shows the impact of the choice of cell technology, all other things being equal. All cells are operated at a current density of 0.5 A/cm2, a pressure of 1 bara, 800 °C, a conversion rate of 70 % and a H_2O/H_2 ratio = 9. It is assumed that changing the operating conditions does not alter the ASR or the degradation rate of the cells. The observed results are essentially the same as in the first part.

➢ Sizing

Table 7 shows the influence of the current density on the overall efficiency of the process and on the sizing of the required stacks. To obtain these results, it extrapolated the ASR up to 1 A/cm2. This assumption is questionable as we observe that the Corre & Brisse stack and the Fang et al. stack seem to be at their linearity limit at 0.4 A/cm2 [22]. The choice between efficiency and required CAPEX depends on a techno-economic analysis.

3.2.2. Influence of Fischer Tropsch reactor operating conditions

➢ Influence of temperature on the global efficiency and on the sizing of Fischer-Tropsch Slurry reactor

The equations describing the kinetics and hydrodynamics of a SBR column were implemented in a Matlab simulation in order to be able to size the reactor according to the operating conditions. The aim is to verify that the conversion rate as a function of the operating conditions is achievable in an industrial-sized reactor. The dimensional limits of an industrial reactor are set at 25 m in height and 5 m in diameter. These values can be compared to the reactor from Sasol's ARGE process (22 m × 5 m) [55].

The Table 8 shows the influence of the temperature on the sizing of the Fischer-Tropsch reactor as a function of operating temperature. The reduction of the temperature has a negative impact on the kinetic rate, but it increases the selectivity toward liquid products and thus reduces the gas flowrate at the reactor inlet (from 19 648 m^3/h to 12 960 m^3/h), moreover, the decrease in temperature allows to increase the concentration of reactant in the reactive liquid phase. Due to these antagonistic effects, the required volume of reactor only increases from 265 m^3 to 783 m^3 when temperature decreases from 240 to 200 °C. The operating conditions provided in the table constitute operating conditions to achieve the desired conversion rate. It should be noted that other conditions would make it possible to obtain this rate, this energy analysis does not make it possible to discriminate the various points of operation allowing the achievement of the objectives. To do this, other criteria must be imposed in a techno-economic analysis.

➢ Product composition of Fischer-Tropsch reactor

The Fig. 10 shows the impact of the reactor temperature on the molecules leaving the reactor, the temperature has a negative impact on the size of the molecules leaving the reactor. It is possible to observe in the Table 8 that the overall efficiency is negatively impacted by the temperature, this phenomenon can be explained by the significant presence of light gas which must be reformed afterwards. The reforming reaction is endothermic and therefore consumes energy to be carried out. The production of molecules heavier than kerosene is regulated using the hydrocracker, but this reactor is exothermic and therefore does not consume energy to operate. It is therefore more efficient to produce molecules heavier than kerosene than lighter ones.

3.2.3. Influence of hydrocracker operating conditions

The model proposed by Gambaro et al. and modified by Sun et al. allows the use of three operating parameters for the Hydrocracker, the temperature between 227 and 242 °C, the mass ratio H_2/wax between 6 and 15 %, and the WHSV between 6 and 12 h^{-1}. Table 9 gives the impact on these parameters on the global efficiency of the system, the selectivity toward jet-fuel and on the catalyst mass required. Increasing the temperature allows to increase the cracking reactions and so reduce the amount of molecules in the range above kerosene in the outlet. This effect is interesting in order to increase efficiency, because it reduces the amount of material that enters the distillation column, an energy-consuming unit. But it increases the cracking of molecules in the kerosene range to the naphtha or LPG fractions and so decreases the selectivity. Because the quantity of matter that comes inside the reactor is lower, it is possible to reduce the amount of catalyst inside the reactor from 25.87 tons to 5.88 tons. Increasing the WHSV rises the amount of catalyst required, because it reduces the conversion rate of the reactor, thus the quantity recycled in the reactor is larger and so it increases the quantity of catalyst required to reach the new WHSV. A higher WHSV

Table 8
Sizing of the column according to the operating temperature.

	200 °C	220 °C	240 °C
Syngas mole fraction in the inlet gas (%)	94.8	93.6	91.8
Mole flow inlet (kmol/h)	6539	7508	9145
Volume flow rate (m^3/h)	12 960	15 506	19 648
Column height (m)	25	25	21.15
Column diameter (m)	5.00	5.00	4.10
Gas velocity (m/s)	0.115	0.191	0.412
Solid concentration	0.38	0.38	0.38
Number of column required	1.60	1.15	1.00
Volume of reactor required (m^3)	783	564	265
Conversion rate (%)	50	50	50
PtL efficiency (%)	49.28	47.21	44.37
Kerosene selectivity (%)	84.36	82.00	78.12

Table 9
Influence of operating parameters on catalyst mass required in HCC, global efficiency and global selectivity.

Influence of temperature			
Temperature	227 °C	242 °C	257 °C
Mass Flow inlet (ton/h)	172.55	57.12	39.23
WHSV (h^{-1})	6.67	6.67	6.67
H_2/Wax (%)	10	10	10
Catalyst mass (ton)	25.87	8.56	5.88
PtL efficiency (%)	44.87	47.21	47.90
Kerosene selectivity (%)	83.36	82.00	80.07
Influence of WHSV			
WHSV	6.67 h^{-1}	9.53 h^{-1}	11.72 h^{-1}
Mass Flow inlet (ton/h)	57.12	97.92	128.39
Temperature (°C)	242	242	242
H_2/Wax (%)	10	10	10
Catalyst mass (ton)	8.56	10.27	10.95
PtL efficiency (%)	47.21	46.47	45.87
Kerosene selectivity (%)	82.00	82.31	82.12
Influence of H_2/wax ratio			
H_2/Wax	6 %	10 %	15 %
Mass Flow inlet (ton/h)	52.28	57.12	79.17
Temperature (°C)	242	242	242
WHSV (h^{-1})	6.53	6.67	7.16
Catalyst mass (ton)	8.01	8.56	11.05
PtL efficiency (%)	47.67	47.21	46.90
Kerosene selectivity (%)	81.85	82.00	82.31

has a negative impact on efficiency without having non-negligible effect on selectivity. Increasing the H_2/Wax mass ratio is positive for selectivity and negative for global efficiency of the system. Increasing this ratio inerts the cracking reaction and so it rises the number of molecules that have to be recycled in the HCC.

3.3. Results of ANOVA

In order to carry out a parametric study of the process, an ANOVA analysis was chosen, this analysis could help to understand between the operating parameters and their interactions, which are significant. A complete 2^6 factorial design (64 runs) was performed in this study. With this design, statistical significance can be checked with respect to the F-tests and p-value. F-tests is the ratio between two variances, and is defined as: $F = \frac{Explained\ variance}{Unexplained\ variance}$. The p-value is defined as the probability of obtaining a result at least as extreme as the results already observed. Operating parameters or the interaction between them are assumed to be significant if their probability value is within the 95 % confidence interval. Table 10 shows the assumed most important parameters (Fischer-Tropsch reactor conversion rate, H_2/CO ratio, reformer reactor conversion rate, Fischer-Tropsch reactor temperature, recycling rate and hydrocracker temperature) and their range selected for the Anova. A minimum temperature of 220 °C is considered, as achieving 60 % of conversion rate at 200 °C would mean working outside the correlation range of the slurry model.

Interaction parameters are tested up to 2nd order interaction and the results are presented in Table 8 in SI and in Fig. 11a and Fig. 11b.

Table 10
Parameters used in ANOVA.

		−1	1
A	**Conversion FT (%)**	30	60
B	**ratio**	1,5	2
C	**Conversion reformer (%)**	30	70
D	**Temperature FT (°C)**	220	240
E	**Recycling (%)**	25	75
F	**Temperature HCC (°C)**	227	257

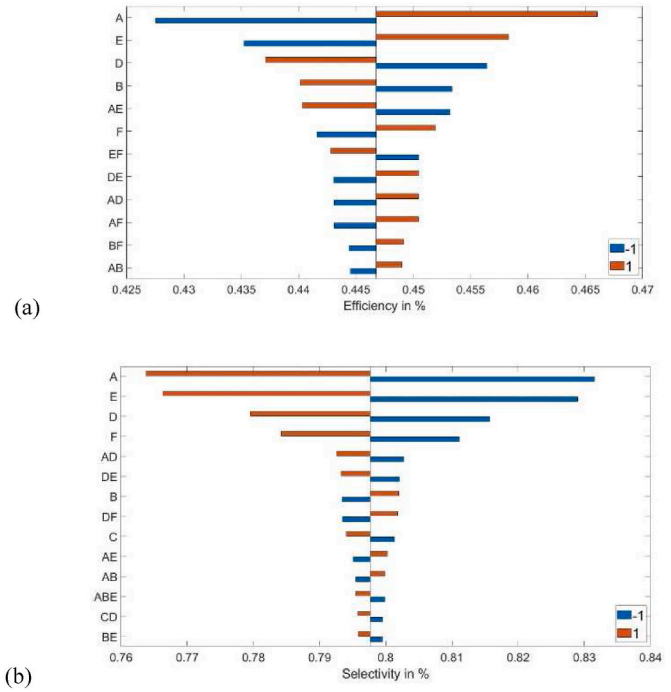

Fig. 11. a: Influence of parameters on global PtL efficiency; b: Influence of parameters on Jet-Fuel selectivity.

The results show all the operating parameters and their interactions that have a significant impact on system performance. Red values are not significant according to the Anova. All parameters significantly influence the selectivity of the process, efficiency is influenced by all the parameters except the conversion rate of the reformer. 7 first-order interactions have a significant impact on efficiency (AB, AD, AE, AF, BF, DE, EF) and 7 have a significant impact on selectivity (AB, AD, AE, BE, CD, DE, DF). A second-order interaction (ABE) has a significant impact on selectivity, which is the interaction between the Fischer-Tropsch reactor conversion rate, the H_2/CO ratio and the recycling rate.

The parameter that most influences the efficiency and selectivity of the process is the conversion rate of the FT reactor. This parameter has a positive impact on efficiency and a negative impact on selectivity. The second more important parameter for efficiency and selectivity is the recycling rate. The increase in the recycling rate is positive for efficiency, and negative for selectivity. The interaction factor between conversion rate and recycling rate was expected. This interaction factor is negative, which means that increasing both the conversion rate and the recycling rate is negative for the efficiency. This behaviour is induced by the increase in light gases at the inlet of the reactor, which reduces the overall efficiency. The third main parameters for both selectivity and efficiency is the temperature of the Fischer-Tropsch reactor. The increase in temperature has a positive impact on efficiency (regardless of whether the increase in temperature induces a higher conversion rate), and also a positive impact on selectivity. The increase in temperature reduces the size of the molecule produced by the Fischer-Tropsch reactor. The consequence of this reduction is an increase in gases that need to be reformed, this operation is one of the main energy consuming operation. The ratio H_2/CO is important primarily for efficiency as it decreases overall efficiency. A lower ratio increases selectivity toward long chain molecules and thus decreases production of LPG. However, an unexpected decrease in selectivity toward kerosene is observed when the ratio decreases, even if this effect is minor compared to other impacts. The temperature of the HCC has a positive impact on efficiency and a negative impact on selectivity. These comportments were predictable, increasing the temperature reduces the quantity of product that had to be separated in the second distillation

column and thus reducing energy consumption. But increasing the temperature increases the cracking of molecules that is not selective, and so increases the production of molecules in a lighter range than kerosene. The conversion rate of the reformer has a low impact on the process by slightly decreasing the overall selectivity.

With significant factors and interaction between them, it is possible to compute PtL efficiency and selectivity with the two following equations:

$$y_{PtL} = 0.4468 + \frac{0.4468}{2} \times (0.0900 \times a - 0.0292 \times b - 0.0423 \times d + 0.0530 \times e + 0.0234 \times f + 0.0101 \times a \times b + 0.0166 \times a \times d - 0.0284 \times a \times e - 0.0116 \times a \times f + 0.0107 \times b \times f + 0.0168 \times d \times e - 0.0170 \times e \times f) \quad (R^2 = 0.9998)$$

$$y_{Selec} = 0.7977 + \frac{0.7977}{2} \times (-0.0875 \times a + 0.0180 \times b - 0.0091 \times c - 0.0443 \times d - 0.0756 \times e - 0.0332 \times f + 0.0056 \times a \times b - 0.0126 \times a \times d - 0.0065 \times a \times e - 0.0046 \times b \times e - 0.0111 \times d \times e + 0.0105 \times d \times f - 0.0055 \times a \times b \times e) \quad (R^2 = 0.9999)$$

With $(a,b,c,d,e,f) \in [-1;1]$, corresponding to the value, in the allowed range, of operating parameter A, B, C, D, E, F. A Power-to-Kerosene function is defined by:

$$y_{Power-to-Kero} = y_{PtL} \times y_{Selec}$$

After using the optimization function of Matlab *fmincon*. An optimal Power-to-Liquid efficiency is found for a Fischer-Tropsch conversion rate of 60 %, a ratio H_2/CO of 1.5, a reformer conversion rate of 30 %, a Fischer-Tropsch temperature of 220 °C, a recycling rate of 75 % and a HCC temperature of 227 °C. The yield calculated by Anova is 48.22 %, the value from the simulation for these parameters is 48.06 %. The same operating conditions with the performance of the Jülich stack could reach a global efficiency of 65.74 %. Further optimization is performed to define the optimal Power-to-Kerosene efficiency. This optimum was found for a conversion rate of 60 %, a H_2/CO ratio of 2.0, a reformer conversion rate of 30 %, a Fischer-Tropsch temperature of 220 °C, a recycling rate of 75 % and HCC temperature of 227 °C. The Power-to-Kerosene efficiency computed by linearisation is 38.59 %, the efficiency estimated by the simulation for these operating conditions is 37.97 % which is lower than the simulated Power-to-kerosene efficiency of the base case (38.71 %).

The influence of operating parameters, analysed one variable at a time, can be observed in Figs. 4–9 in SI. These graphs primarily provide information similar to that of the ANOVA regarding the most influential parameters on the process, particularly in terms of efficiency and selectivity. However, this analysis also yields some noteworthy insights.

The H2/CO ratio does not linearly influence efficiency, which peaks at a ratio of approximately 1.8. This optimum could be attributed to a trade-off between the limitation in the system of unreacted CO when the stoichiometry is closer to 2, and a decrease in methane production with a lower ratio. Furthermore, the increase in efficiency with the conversion rate of the Fischer-Tropsch reactor appears to plateau when the conversion rate exceeds 60 %. According to the ANOVA, the influence of the reformer conversion on process efficiency is presumed to be negligible. However, the one-variable-at-a-time study indicates that this influence is quite significant. The conversion rate increases from 46.38 % to 48.48 % when the methane conversion rate in the reformer rises from 30 % to 70 %.

3.4. Comparison with literature data

To our knowledge, the only data available in the scientific literature for a pilot Power to Liquid process comes from the SOLETAIR project [56]. This project was a Power to Liquid proof-of-concept demonstrator with a power consumption of 5.60 kW. This work is the first to propose an energy analysis of the Power to Jet-Fuel process, although other simulations studies exist in the literature to estimate the energy analysis of a Power-to-Liquid based on Fischer Tropsch, that are presented in a non-exhaustive way in the Table 11.

The results with an ESC are slightly lower than the value of the previous studies. This result is explained by the LTFT conversion rate, which is lower in this study than in most other studies, and by the use of a distillation column. This one is required to obtain a product quality compatible with ASTM regulations. The results of Adelung et al. and Roja-Michaga et al. are much lower than the other values, which can be explained by the use of low temperature electrolyzer in these studies. A SOEC allows the recycling of a large quantity of heat provided by the Fischer-Tropsch reactor to the production of hydrogen.

The result with a CSC presented in the table is superior to most other efficiencies proposed in the literature. This efficiency is higher due to the high performance of this technology. In order to obtain these results, the performance value of a cathode supported cell provided by Fang et al. was used. Kulkarni et al. proposed a process that achieved the highest efficiency, which can be attributed to the high conversion rate of HTFT (82 %) and the absence of strict separation units. The efficiency achieved in Delgado et al.'s paper is also higher. This difference could be due to the fact that the authors did not crack both wax and diesel in their study, instead considering diesel as a product. Peter et al.'s article proposed a process that is quite similar to the one in this study. The efficiency results are comparable, with 52.1 % in their study versus 48.06 % in this one. The efficiency of the electrolyzer in this study (80 %) is quite similar to our base case with ESC (78.11 %). This study also differs in terms of the final product considered. Kerosene and diesel are the final products in their study and naphtha is reformed. However in this study, the final products considered are naphtha and kerosene. These two differences could explain the slight variations between the two studies.

4. Conclusions

In this publication an energy analysis of the Power-to-Liquid process has been performed. To do so, a complete simulation of the plant was performed. Separators, pumps, compressors and equilibrium reactors were simulated using Aspen Hysys, while more complex elements such as the Fischer-Tropsch reactor, hydrocracker and SOEC were simulated using Matlab. All of this simulation allowed the analysis of the energy efficiency of a plant oriented towards the production of Jet-Fuel respecting all the ASTM specifications. The purpose of the study is to present this analysis through high TRL technologies and so already accessible technologies.

The system reaches a global efficiency of 48.06 % in the most efficient operating conditions and could reach up to 38.71 % of Power-to-Kerosene efficiency. If the market could not absorb Naphtha as a coproduct, it is possible to produce exclusively Jet-Fuel with an efficiency of 43.73 %. This result is reached with values from a commercial electrolyte supported stack. Even if the TRL is lower, values from a more efficient cathode supported stack have been also considered, it is possible to increase global efficiency up to 64.25 % and Power to kerosene efficiency to 52.68 %. This value gives an insight on the future efficiency that could be reasonably expected from a commercial stack in the following years.

The values provided in this section should be interpreted with caution due to the limitations of the model. The efficiency of the SOEC is extrapolated from data obtained from a small unit to a large industrial plant. Additionally, its assumed that the degradation evolves linearly over time. The Fischer-Tropsch product distribution is derived from Vervloet et al. modified with data from Pandey et al. for ethane and methane selectivity. Although the fitting of these values is reasonably acceptable, uncertainties exist. The actual product distribution may differ from the simulated one, which could alter the overall selectivity

Table 11
Comparison between this study and other power-to-Liquid studies.

Study	Electrolyser	Fischer Tropsch Reactor (Conv. Per pass)	Tail gas valorisation	Product separation	Product upgrading	LHV efficiency (%)
Adelung *et al.* [17]	PEM	LTFT – 40 %	Burner	8 Flash	HCC	38.7
Becker *et al.* [57]	SOEC + Co-Electrolysis	LTFT – 80 %	Burner	Distillation	HCC + Catalytic reforming + C5/C6 isomerisation	51
Cinti *et al.* [18]	SOEC + Co-Electrolysis	LTFT – 87 %	Reformer	No separator	No upgrading	57.2
Pratschner *et al.* [58]	SOEC + Co-Electrolysis	LTFT – 55 %	Reformer + Burner	3 Flash	No upgrading	62.7
Gao *et al.* [59]	SOEC + Co-Electrolysis	HTFT	SNG as a product	2 Flash + 1 decanter	No upgrading	54.26
Kulkarni *et al.* [60]	SOEC + Co-Electrolysis	HTFT – 82 %	Burner	4 Flash separator	No upgrading	68
König *et al.* [61]	PEM	LTFT – 40 %	Burner	6 Flash separators	HCC	44.6
Herz *et al.* [62]	SOEC + Co-Electrolysis	LTFT – 80 %	Burner	2 Flash separators	No upgrading	68
Roja-Michaga *et al.* [12]	Alkaline	LTFT – 75 %	Burner	Distillation	HCC	28.06
Tanaka *et al.* [63]	SOEC + Co-Electrolysis	n.a. – 78 %	No gas product	No separator	No upgrading	58.6
Delgado et *al.* [64]	SOEC	LTFT – 52.2 %	Burner	Distillation	HCC	69.8
Sanchez-Lujan *et al.* [65]	SOEC – Co-Electrolysis	LTFT - >75 %	POX	3 Flash separators	No upgrading	49
Peters *et al.* [66]	SOEC – Co-electrolysis	LTFT – 80 %	Reformer	Distillation	HCC	52.1
Markowitsch *et al.* (scenario 9) [67]	SOEC	LTFT – 40 %	Reformed in RWGS	2 Flash separators	No upgrading	53.9
This study	SOEC (Current ESC)	LTFT – 60 %	Reformer	Distillation	HCC	48.06
This study	SOEC (Future CSC)	LTFT – 60 %	Reformer	Distillation	HCC	64.25

and efficiency. Lastly, the hydrocracker simulation is based on values obtained from a small experimental test bench. Therefore, extrapolating these results to an industrial-sized reactor may not yield accurate results.

The results here are not considering co-electrolysis, even if this technology could greatly improve efficiency of the plant, it is difficult to find ASR and degradation rate of stack with CO_2 reduction. Co-electrolysis is a compelling technology due to its ability to directly reduce carbon dioxide in the same unit as steam. This process eliminates energy loss that typically occurs between hydrogen production and the reverse water gas shift unit, thereby reducing the capital expenditure. The result presented here is provided for a large-scale production (200 MW of electrolyser) producing steady-state kerosene and naphtha, requiring constant electrical consumption.

Declaration of competing interest

The authors declare that they have no known competing financial interests or personal relationships that could have appeared to influence the work reported in this paper.

Appendix A. Supplementary data

Supplementary data to this article can be found online at https://doi.org/10.1016/j.ijhydene.2024.01.262.

References

[1] United Nations Framework Convention on Climate Change. Paris agreement. 2015.
[2] IPCC. Global warming of 1.5°C an IPCC Special Report on the impacts of global warming of 1.5°C above pre-industrial levels and related global greenhouse gas emission pathways,in the context of strengthening the global response to the threat of climate change, sustainable development, and efforts to eradicate poverty. 2019.
[3] AR5 Climate Change 2014: Mitigation of Climate Change — IPCC n.d. https://www.ipcc.ch/report/ar5/wg3/(accessed March 15, 2022).
[4] Greenhouse gas emissions from transport in Europe — European Environment Agency n.d. https://www.eea.europa.eu/data-and-maps/indicators/transport-emissions-of-greenhouse-gases/transport-emissions-of-greenhouse-gases-12 (accessed March 15, 2022).
[5] Sharmina M, Edelenbosch OY, Wilson C, Freeman R, Gernaat DEHJ, Gilbert P, et al. Decarbonising the critical sectors of aviation, shipping, road freight and industry to limit warming to 1.5–2°C. Clim Pol 2021;21:455–74. https://doi.org/10.1080/14693062.2020.1831430.
[6] IATA. Carbon offsetting for international aviation. 2020.
[7] ICAO. Conference ON AVIATION and alternative fuels. 2017.
[8] ATAG. Waypoint 2050. Balancing growth in connectivity with a comprehensive global air transport response to the climate emergency: a vision of net-zero aviation by mid-century. 2021.
[9] Moustakidis S. Renewable energy – Recast to 2030 (RED II). EU Science Hub - European Commission; 2018. https://ec.europa.eu/jrc/en/jec/renewable-energy-recast-2030-red-ii. [Accessed 2 December 2021].
[10] CSIRO. Opportunities for hydrogen in commercial aviation n.d. https://www.csiro.au/en/work-with-us/services/consultancy-strategic-advice-services/csiro-futures/futures-reports/energy-and-resources/hydrogen-commercial-aviation (accessed March 16, 2022).
[11] Standard Specification for Aviation Turbine Fuel Containing Synthesized Hydrocarbons n.d. https://www.astm.org/d7566-21.html (accessed March 16, 2022).
[12] Rojas-Michaga MF, Michailos S, Cardozo E, Akram M, Hughes KJ, Ingham D, et al. Sustainable aviation fuel (SAF) production through power-to-liquid (PtL): a combined techno-economic and life cycle assessment. Energy Convers Manag 2023;292:117427. https://doi.org/10.1016/j.enconman.2023.117427.
[13] Robinson PR, Hsu CS. Introduction to petroleum technology. In: Hsu CS, Robinson PR, editors. Springer Handbook of petroleum technology. Cham: Springer International Publishing; 2017. p. 1–83. https://doi.org/10.1007/978-3-319-49347-3_1.
[14] NIST Chemistry WebBook n.d.
[15] Streed GG. Vapor-liquid equilibria for high temperatur, high pressure hydrogen – hydrocarbon systems. OnePetro; 1963.
[16] Roussanaly S, Fu C, Voldsund M, Anantharaman R, Spinelli M, Romano M. Techno-economic analysis of MEA CO2 capture from a cement Kiln – impact of steam supply scenario. Energy Proc 2017;114:6229–39. https://doi.org/10.1016/j.egypro.2017.03.1761.
[17] Adelung S, Maier S, Dietrich R-U. Impact of the reverse water-gas shift operating conditions on the Power-to-Liquid process efficiency. Sustain Energy Technol Assessments 2021;43:100897. https://doi.org/10.1016/j.seta.2020.100897.
[18] Cinti G, Baldinelli A, Di Michele A, Desideri U. Integration of solid oxide electrolyzer and Fischer-tropsch: a sustainable pathway for synthetic fuel. Appl Energy 2016;162:308–20. https://doi.org/10.1016/j.apenergy.2015.10.053.
[19] Udagawa J, Aguiar P, Brandon NP. Hydrogen production through steam electrolysis: model-based steady state performance of a cathode-supported intermediate temperature solid oxide electrolysis cell. J Power Sources 2007;166:127–36. https://doi.org/10.1016/j.jpowsour.2006.12.081.
[20] Alenazey F, Alyousef Y, Almisned O, Almutairi G, Ghouse M, Montinaro D, et al. Production of synthesis gas (H2 and CO) by high-temperature Co-electrolysis of

H2O and CO2. Int J Hydrogen Energy 2015;40:10274–80. https://doi.org/10.1016/j.ijhydene.2015.06.034.
[21] Corre G, Brisse A. 9000 hours operation of a 25 solid oxide cells stack in steam electrolysis mode. ECS Trans 2015;68:3481. https://doi.org/10.1149/06801.3481ecst.
[22] Fang Q, Frey CE, Menzler NH, Blum L. Electrochemical performance and preliminary post-mortem analysis of a solid oxide cell stack with 20,000 h of operation. J Electrochem Soc 2018;165:F38. https://doi.org/10.1149/2.0541802jes.
[23] Yan Y, Fang Q, Blum L, Lehnert W. Performance and degradation of an SOEC stack with different cell components. Electrochim Acta 2017;258:1254–61. https://doi.org/10.1016/j.electacta.2017.11.180.
[24] Rinaldi G, Diethelm S, Oveisi E, Burdet P, Van herle J, Montinaro D, et al. Post-test analysis on a solid oxide cell stack operated for 10,700 hours in steam electrolysis mode. Fuel Cell 2017;17:541–9. https://doi.org/10.1002/fuce.201600194.
[25] Mougin J, Iorio SD, Chatroux A, Donnier-Marechal T, Palcoux G, Petitjean M, et al. Development of a solid oxide electrolysis stack able to operate at high steam conversion rate and integration into a SOE system. ECS Trans 2017;78:3065. https://doi.org/10.1149/07801.3065ecst.
[26] Lang M, Raab S, Lemcke MS, Bohn C, Pysik M. Long term behavior of solid oxide electrolyser (SOEC) stacks. ECS Trans 2019;91:2713. https://doi.org/10.1149/09101.2713ecst.
[27] Königshofer B, Boškoski P, Nusev G, Koroschetz M, Hochfellner M, Schwaiger M, et al. Performance assessment and evaluation of SOC stacks designed for application in a reversible operated 150 kW rSOC power plant. Appl Energy 2021;283:116372. https://doi.org/10.1016/j.apenergy.2020.116372.
[28] Zheng Y, Li Q, Guan W, Xu C, Wu W, Wang WG. Investigation of 30-cell solid oxide electrolyzer stack modules for hydrogen production. Ceram Int 2014;40:5801–9. https://doi.org/10.1016/j.ceramint.2013.11.020.
[29] Nuggehalli Sampathkumar S, Aubin P, Couturier K, Sun X, Sudireddy BR, Diethelm S, et al. Degradation study of a reversible solid oxide cell (rSOC) short stack using distribution of relaxation times (DRT) analysis. Int J Hydrogen Energy 2022;47:10175–93. https://doi.org/10.1016/j.ijhydene.2022.01.104.
[30] Kusnezoff M, Jahn M, Megel S, Reichelt E, Trofimenko N, Herz G, et al. Progress in SOC development at fraunhofer IKTS. ECS Trans 2021;103:307. https://doi.org/10.1149/10301.0307ecst.
[31] Hauch A, Ploner A, Pylypko S, Cubizolles G, Mougin J. Test and characterization of reversible solid oxide cells and stacks for innovative renewable energy storage. Fuel Cell 2021;21:467–76. https://doi.org/10.1002/fuce.202100046.
[32] Riedel M, Heddrich MP, Friedrich KA. Analysis of pressurized operation of 10 layer solid oxide electrolysis stacks. Int J Hydrogen Energy 2019;44:4570–81. https://doi.org/10.1016/j.ijhydene.2018.12.168.
[33] Cui X, Kær SK. Thermodynamic analysis of steam reforming and oxidative steam reforming of propane and butane for hydrogen production. Int J Hydrogen Energy 2018;43:13009–21. https://doi.org/10.1016/j.ijhydene.2018.05.083.
[34] Almind MR, Vendelbo SB, Hansen MF, Vinum MG, Frandsen C, Mortensen PM, et al. Improving performance of induction-heated steam methane reforming. Catal Today 2020;342:13–20. https://doi.org/10.1016/j.cattod.2019.05.005.
[35] Ma J, Jiang B, Gao Y, Yu K, Lv Z, Si-ma W, et al. A compact and high-efficiency electrified reactor for hydrogen production by methane steam reforming. Int J Hydrogen Energy 2022;47:41421–31. https://doi.org/10.1016/j.ijhydene.2022.04.281.
[36] Rytter E, Holmen A. Deactivation and regeneration of commercial type fischer-tropsch Co-Catalysts—a mini-review. Catalysts 2015;5:478–99. https://doi.org/10.3390/catal5020478.
[37] Maretto C, Krishna R. Modelling of a bubble column slurry reactor for Fischer–Tropsch synthesis. Catal Today 1999;52:279–89. https://doi.org/10.1016/S0920-5861(99)00082-6.
[38] Krishna R, Ellenberger J, Sie ST. Reactor development for conversion of natural gas to liquid fuels: a scale-up strategy relying on hydrodynamic analogies. Chem Eng Sci 1996;51:2041–50. https://doi.org/10.1016/0009-2509(96)00061-9.
[39] Krishna R, Ellenberger J. Gas holdup in bubble column reactors operating in the churn-turbulent flow regime - Krishna - 1996. AIChE Journal - Wiley Online Library; 1996. https://doi.org/10.1002/aic.690420923. 2627–34.
[40] Krishna R, De Swart JWA, Ellenberger J, Martina GB, Maretto C. Gas holdup in slurry bubble columns: effect of column diameter and slurry concentrations. AIChE J 1997;43:311–6. https://doi.org/10.1002/aic.690430204.
[41] Letzel HM, Schouten JC, van den Bleek CM, Krishna R. Influence of elevated pressure on the stability of bubbly flows. Chem Eng Sci 1997;52:3733–9. https://doi.org/10.1016/S0009-2509(97)00219-4.
[42] De Swart JWA, van Vliet RE, Krishna R. Size, structure and dynamics of “large” bubbles in a two-dimensional slurry bubble column. Chem Eng Sci 1996;51:4619–29. https://doi.org/10.1016/0009-2509(96)00265-5.
[43] Yates IC, Satterfield CN. Intrinsic kinetics of the Fischer-Tropsch synthesis on a cobalt catalyst. Energy Fuels 1991;5:168–73. https://doi.org/10.1021/ef00025a029.
[44] Vervloet D, Kapteijn F, Nijenhuis J, Ommen JR van. Fischer–Tropsch reaction–diffusion in a cobalt catalyst particle: aspects of activity and selectivity for a variable chain growth probability. Catal Sci Technol 2012;2:1221–33. https://doi.org/10.1039/C2CY20060K.
[45] Pandey U, Runningen A, Gavrilović L, Jørgensen EA, Putta KR, Rout KR, et al. Modeling Fischer–Tropsch kinetics and product distribution over a cobalt catalyst. AIChE J 2021;67:e17234. https://doi.org/10.1002/aic.17234.
[46] Gu W, Wang K, Huang Y, Zhang B, Chen Q, Hui C-W. Energy optimization for a multistage crude oil distillation process. Chem Eng Technol 2015;38:1243–53. https://doi.org/10.1002/ceat.201400130.
[47] Fraser S. In: Górak Andrzej, Schoenmakers Hartmut, editors. Chapter 4 - distillation in refining. Distillation. Academic Press; 2014.
[48] Song W, Mahalec V, Long J, Yang M, Qian F. Modeling the hydrocracking process with deep neural networks. Ind Eng Chem Res 2020;59:3077–90. https://doi.org/10.1021/acs.iecr.9b06295.
[49] Mohanty S, Kunzru D, Saraf DN. Hydrocracking: a review. Fuel 1990;69:1467–73. https://doi.org/10.1016/0016-2361(90)90192-S.
[50] Bhutani N, Ray AK, Rangaiah GP. Modeling, simulation, and multi-objective optimization of an industrial hydrocracking unit. Ind Eng Chem Res 2006;45:1354–72. https://doi.org/10.1021/ie050423f.
[51] Gambaro C, Calemma V, Molinari D, Denayer J. Hydrocracking of Fischer-Tropsch waxes: kinetic modeling via LHHW approach. AIChE J 2011;57:711–23. https://doi.org/10.1002/aic.12291.
[52] Sun C, Luo Z, Choudhary A, Pfeifer P, Dittmeyer R. Influence of the condensable hydrocarbons on an integrated fischer–tropsch synthesis and hydrocracking process: simulation and experimental validation. Ind Eng Chem Res 2017;56:13075–85. https://doi.org/10.1021/acs.iecr.7b01326.
[53] Marano JJ, Holder GD. Characterization of Fischer-Tropsch liquids for vapor-liquid equilibria calculations. Fluid Phase Equil 1997;138:1–21. https://doi.org/10.1016/S0378-3812(97)00166-0.
[54] de Klerk A. Fischer–Tropsch fuels refinery design. Energy Environ Sci 2011;4:1177–205. https://doi.org/10.1039/C0EE00692K.
[55] Krishna R, Sie ST. Design and scale-up of the Fischer–Tropsch bubble column slurry reactor. Fuel Process Technol 2000;64:73–105. https://doi.org/10.1016/S0378-3820(99)00128-9.
[56] Vázquez FV, Koponen J, Ruuskanen V, Bajamundi C, Kosonen A, Simell P, et al. Power-to-X technology using renewable electricity and carbon dioxide from ambient air: SOLETAIR proof-of-concept and improved process concept. J CO2 Util 2018;28:235–46. https://doi.org/10.1016/j.jcou.2018.09.026.
[57] Becker WL, Braun RJ, Penev M, Melaina M. Production of Fischer–Tropsch liquid fuels from high temperature solid oxide co-electrolysis units. Energy 2012;47:99–115. https://doi.org/10.1016/j.energy.2012.08.047.
[58] Pratschner S, Hammerschmid M, Müller FJ, Müller S, Winter F. Simulation of a pilot scale power-to-liquid plant producing synthetic fuel and wax by combining fischer–tropsch synthesis and SOEC. Energies 2022;15:4134. https://doi.org/10.3390/en15114134.
[59] Gao R, Zhang L, Wang L, Zhang X, Zhang C, Jun K-W, et al. A comparative study on hybrid power-to-liquids/power-to-gas processes coupled with different water electrolysis technologies. Energy Convers Manag 2022;263:115671. https://doi.org/10.1016/j.enconman.2022.115671.
[60] Kulkarni A P, Hos T, Landau M V, Fini D, Giddey S, Herskowitz M. Techno-economic analysis of a sustainable process for converting CO 2 and H 2 O to feedstock for fuels and chemicals. Sustain Energy Fuels 2021;5:486–500. https://doi.org/10.1039/D0SE01125H.
[61] König DH, Freiberg M, Dietrich R-U, Wörner A. Techno-economic study of the storage of fluctuating renewable energy in liquid hydrocarbons. Fuel 2015;159:289–97. https://doi.org/10.1016/j.fuel.2015.06.085.
[62] Herz G, Reichelt E, Jahn M. Techno-economic analysis of a co-electrolysis-based synthesis process for the production of hydrocarbons. Appl Energy 2018;215:309–20. https://doi.org/10.1016/j.apenergy.2018.02.007.
[63] Tanaka Y, Yamaji K, Ishiyama T. Co-electrolysis performance and process analyses for synthetic liquid fuel production. ECS Trans 2023;111:1947. https://doi.org/10.1149/11106.1947ecst.
[64] Delgado HE, Cappello V, Zang G, Sun P, Ng C, Vyawahare P, et al. Techno-economic analysis and life cycle analysis of e-fuel production using nuclear energy. J CO2 Util 2023;72:102481. https://doi.org/10.1016/j.jcou.2023.102481.
[65] Sánchez-Luján J, Molina-García Á, López-Cascales JJ. Optimal integration modeling of Co – electrolysis in a power-to-liquid industrial process. Int J Hydrogen Energy 2024;52:1202–19. https://doi.org/10.1016/j.ijhydene.2023.07.012.
[66] Peters R, Wegener N, Samsun RC, Schorn F, Riese J, Grünewald M, et al. A techno-economic assessment of fischer–tropsch fuels based on syngas from Co-electrolysis. Processes 2022;10:699. https://doi.org/10.3390/pr10040699.
[67] Markowitsch C, Lehner M, Maly M. Evaluation of process structures and reactor technologies of an integrated power-to-liquid plant at a cement factory. J CO2 Util 2023;70:102449. https://doi.org/10.1016/j.jcou.2023.102449.